Climate Dynamics (2025) 63:374
https://doi.org/10.1007/s00382-025-07878-3

ORIGINAL ARTICLE

Drivers of summer Antarctic sea-ice extent at interannual time scale in CMIP6 large ensembles based on information flow

David Docquier[1] · François Massonnet[2] · Benjamin Richaud[2] · Thierry Fichefet[2] · Hugues Goosse[2] · Bianca Mezzina[2] · Dániel Topál[2] · Stéphane Vannitsem[1,3]

Received: 7 March 2025 / Accepted: 7 September 2025

Abstract
The trend in Antarctic sea-ice extent has been slightly positive between 1979 and 2015. However, a series of record lows in Antarctic sea ice have occurred since 2016, especially during summer, which could indicate a regime shift. In this context, it is of crucial importance to better understand the drivers of changes in summer Antarctic sea-ice extent. In our study, we make use of five different large model ensembles and compute cause-effect relationships between variables based on the Liang-Kleeman information flow method at the interannual time scale over the period 1970–2100. We find that proximate factors, such as the previous spring sea-ice extent, sea-surface temperature and surface air temperature, are generally the most important drivers of changes in summer Antarctic sea-ice extent at the pan-Antarctic scale, as well as in most Antarctic sectors. The Southern Annular Mode (SAM), Amundsen Sea Low (ASL), and teleconnection patterns associated with El Niño-Southern Oscillation (ENSO) and Indian Ocean Dipole (IOD) also have direct and indirect influences on summer sea-ice extent, but with a generally weaker impact compared to proximate factors. An exception is the Western Pacific Ocean, where ENSO and IOD play the largest role. The Indian and Western Pacific Oceans generally present fewer causal connections compared to the Bellingshausen-Amundsen, Weddell and Ross Seas, partly leading to smaller values of direct causal influences on summer sea-ice extent, which indicates a more unpredictable behavior of sea ice in these two sectors.

Keywords Antarctic sea ice · Causality · Information flow · CMIP6 models · Large ensembles

1 Introduction

The total Antarctic sea-ice extent slightly increased from 1979 to 2015 (Turner et al. 2015; Maksym 2019). Afterwards, a sudden decrease in sea-ice extent occurred in spring-summer 2016–2017 (Stuecker et al. 2017; Eayrs et al. 2021; Zhang et al. 2022; Mezzina et al. 2024a), followed by a series of low values of sea-ice extent since then, especially in summer (Purich and Doddridge 2023; Zhang and Li 2023; Gilbert and Holmes 2024; Wang et al. 2024). The year 2023 was exceptional in that not only the summer minimum sea-ice extent reached a record low (Purich and Doddridge 2023), but also the winter maximum was the lowest on record in the satellite era, following a very slow sea-ice growth in autumn and winter (Gilbert and Holmes 2024; Jena et al. 2024; Roach and Meier 2024). The year 2024 followed a similar trend, with summer minimum and winter maximum only slightly above the record low values of 2023 (OSI SAF 2023; Comiso et al. 2024). These recent changes altogether have raised the question of whether Antarctic sea ice has undergone a regime shift (Fogt et al. 2022; Hobbs et al. 2024; Raphael et al. 2025).

In this context, understanding the causes of the recent changes in Antarctic sea-ice extent is of prime importance as these changes affect polar and global climates (Zhou et al. 2023; Liu and Zhu 2024) as well as marine and coastal ecosystems (Swadling et al. 2023). Beyond the classical (and important) question of whether these changes are either

✉ David Docquier
david.docquier@meteo.be

1 Royal Meteorological Institute of Belgium, Brussels, Belgium

2 Earth and Life Institute, Université catholique de Louvain, Louvain-la-Neuve, Belgium

3 Division of Frontier Research, Southern Marine Laboratory, Zhuhai, China

Published online: 06 October 2025

externally (mainly via human greenhouse gas emissions) or internally driven (Morioka et al. 2024b), it is also crucial to try to understand the key processes at play and the interactions between the different climate variables. Both the atmosphere and ocean drive changes in Antarctic sea ice, with the atmosphere typically influencing sea ice at shorter time scales, while the ocean generally acts at longer time scales (Hobbs et al. 2024).

The Southern Annular Mode (SAM), which is the dominant mode of atmospheric variability in the extra-tropical Southern Hemisphere (Gong and Wang 1999; Marshall 2003), varies with the strength of westerly winds that encircle Antarctica (with positive SAM when winds are stronger, and negative SAM when winds are weaker). These changes in SAM can have an important impact on Antarctic sea ice (Doddridge and Marshall 2017). For example, a positive SAM brings more cyclonic conditions in the South Pacific sector of the Southern Ocean (Amundsen Sea Low [ASL] deepening), which typically decreases sea-ice extent in the Bellingshausen Sea and increases it in the Ross Sea (Lefebvre et al. 2004; Turner et al. 2015; Zhang and Li 2023). However, the SAM influence depends on the time scale considered (Ferreira et al. 2015) and can be modulated by El Niño-Southern Oscillation (ENSO; Ding et al. 2012; Maksym 2019; Wang et al. 2023) and zonal wave 3 patterns (Eabry et al. 2024). The Indian Ocean Dipole (IOD) may also exert some indirect influence on Antarctic sea ice via the excitation of poleward Rossby wave trains (Zhang et al. 2024). An influence of the Interdecadal Pacific Oscillation (IPO) on Antarctic sea ice has also been found in several studies (e.g. Bonan et al. 2024).

Although the relationship between Antarctic sea ice and surface air temperature is complicated when considering the pan-Antarctic scale and the relatively short observational time period, higher temperatures generally lead to reduced sea-ice extent at the regional scale (Shu et al. 2012) and future model projections show a declining Antarctic sea-ice extent in a warmer world (Fox-Kemper et al. 2021). The ocean also drives changes in Antarctic sea ice. Observational evidence suggests that increased upwelling warm water played a role in the large sea-ice reduction in spring 2016 (Meehl et al. 2019). The influence of subsurface warming of the Southern Ocean was also confirmed in the record low sea-ice summer minimum of 2023 (Purich and Doddridge 2023). Additionally, the sea-ice state in preceding seasons is a skillful predictor of the next summer sea-ice extent since 2010 (Hobbs et al. 2024).

Despite the relatively large range of studies investigating the causes of recent changes in summer Antarctic sea ice, many uncertainties remain regarding the relative importance of each driver, as well as their potential direct or indirect influence. That is why we try to go a step beyond in this analysis and quantify cause-effect relationships between variables, including the identification of indirect causal links.

A key metric that has been traditionally used in climate studies to infer causal relationships between variables is (lagged) correlation. However, correlation does not necessarily imply causation, as a statistically significant correlation between two variables could be the result of an external third variable that influences both variables (Sugihara et al. 2012; Liang 2014; Runge et al. 2023; Docquier et al. 2024a). Other limitations related to the use of correlation are the impossibility to identify the causal direction and the restricted use on pairs of variables. For these different reasons, causal methods have been employed more and more in Earth science (Runge et al. 2019), as they allow to quantify cause-effect relationships between variables.

The Liang-Kleeman information flow method is particularly interesting as it is directly derived from the first principles of information theory and translates into a relatively simple expression based on covariances between the different pairs of variables that are considered (Liang and Kleeman 2005; Liang 2014, 2016, 2021). This causal method has been used in several climate studies, e.g. for analyzing the interactions between Antarctic ice-sheet surface mass balance, surface air temperature, sea-ice concentration, SAM and ENSO (Vannitsem et al. 2019), the connection between Antarctic mean isotopic composition of ice cores, sea-ice area and teleconnection patterns (Vannitsem et al. 2025), the drivers of Arctic sea ice (Docquier et al. 2022, 2024b), the carbon dioxide—surface air temperature relationship (Hagan et al. 2022), or the sea-surface temperature—precipitation relationship (Ye and Tozuka 2022).

In this study, we investigate the role of atmospheric and ocean drivers of summer Antarctic sea-ice extent at interannual time scale using five different large ensembles participating in the Coupled Model Intercomparison Project Phase 6 (CMIP6), which we compare to observational and reanalysis datasets. We quantify the cause-effect relationships between the different variables analyzed using the Liang-Kleeman information flow method. To the best of our knowledge, it is the first time that a causal method has been used to investigate drivers of Antarctic sea-ice changes. We focus our analysis on the recent past and twenty-first century (1970–2100) and we look at different Antarctic sectors, as we know that Antarctic sea-ice variability is spatially heterogeneous. Our approach differs from previous studies that investigate specific events, such as the recent sea-ice lows, by looking at drivers of change over the whole period instead. Section 2 provides details about the Antarctic sectors used here (Sect. 2.1), the climate models (Sect. 2.2) and reference products (satellite observations and reanalyses; Sect. 2.3), as well as the Liang-Kleeman information

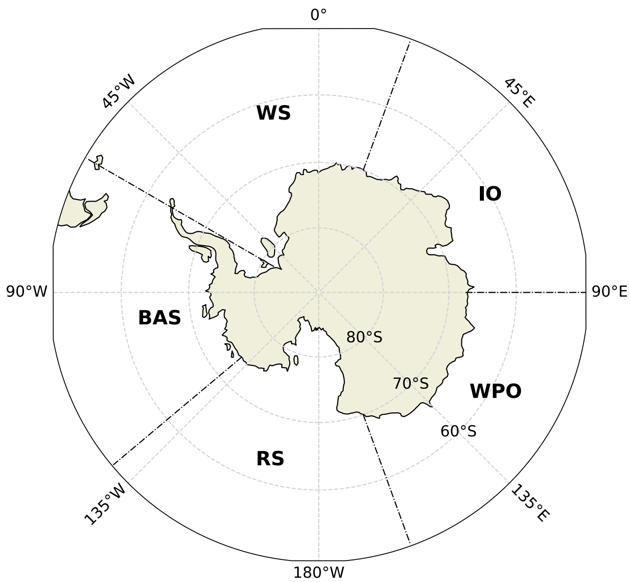

Fig. 1 Antarctic sectors following Zwally et al. (1983). BAS: Bellingshausen-Amundsen Seas (130°W–60°W); WS: Weddell Sea (60°W–20°E); IO: Indian Ocean (20°E–90°E); WPO: Western Pacific Ocean (90°E–160°E); RS: Ross Sea (160°E–130°W)

flow method (Sect. 2.4). In Sect. 3, we provide the main results of our study at the pan-Antarctic scale (Sect. 3.1), as well as for the different Antarctic sectors (Sect. 3.2). Section 4 discusses our results in light of the previous literature (Sect. 4.1), highlights regional differences (Sect. 4.2) and the dependence of our results on the model used (Sect. 4.3), and provides a discussion of advantages and limitations of the causal method (Sect. 4.4). Section 5 concludes our analysis.

2 Methods

2.1 Antarctic sectors

Due to the relatively large spatial heterogeneity in Antarctic sea-ice variability since 1979 (Raphael and Hobbs 2014), we not only look at the pan-Antarctic scale, but also perform a regional analysis. Several definitions for dividing Antarctic sea ice into different sectors exist, the two main definitions being based either on geography (Zwally et al. 1983) or on sea-ice concentration variability (Raphael and Hobbs 2014). In our study, we choose the former definition (Fig. 1; Zwally et al. 1983), which divides Antarctic sea ice into five different sectors: Bellingshausen-Amundsen Seas (130°W–60°W), Weddell Sea (60°W–20°E), Indian Ocean (20°E–90°E), Western Pacific Ocean (90°E–160°E), and Ross Sea (160°E–130°W). This definition is the most widely used in the literature, which makes it easier to compare to previous studies. Another advantage with this definition is that it divides the Southern Ocean into sectors of relatively similar area. For both the pan-Antarctic scale and the Antarctic sectors, the northern limit for the computation of sea-ice extent is 50°S and the one for mean surface air temperature and sea-surface temperature (SST) is 60°S.

2.2 Climate models

In our study, we use five different large ensembles (Table 1) that were run with the same forcing from the Coupled Model Intercomparison Project Phase 6 (CMIP6; Eyring et al. 2016), from which we retrieve monthly mean model outputs. Our analysis period is from 1970 (start date of EC-Earth3 large ensemble) to 2100. We make use of CMIP6 historical forcing from 1970 to 2014, and Shared Socio-economic Pathway 3−7.0 (SSP3−7.0) from 2015 to 2100. The latter scenario is chosen because it is the only scenario that was run by the CESM2 model. Four models have 50

Table 1 Large ensembles used in this study

Model	Members	Atm. model	Atm. resolution	Ocean-SI model	Ocean resolution
ACCESS-ESM1.5 (Ziehn et al. 2019a, b, 2020)	40	UM	1.875° × 1.25° (70 km)	MOM5-CICE4	1° (40 km)
CanESM5 (Swart et al. 2019a, b, c)	50	CanAM5	2.8° (110 km)	NEMO3.4-LIM2	1° (40 km)
CESM2 (Rodgers et al. 2021)	50	CAM6	1° (50 km)	POP2-CICE5	1° (40 km)
EC-Earth3 (EC-Earth-Consortium 2019a, b; Wyser et al. 2021)	50	IFS cy36r4	0.7° (30 km)	NEMO3.6-LIM3	1° (40 km)
MPI-ESM1.2-LR (Wieners et al. 2019a, b; Olonscheck et al. 2023)	50	ECHAM6	1.8° (70 km)	MPIOM	1.5° (50 km)

References are provided for each model, along with the number of members used here, the atmospheric (atm.) model and its nominal resolution, and the ocean-sea ice (ocean-SI) model and its nominal resolution. The resolution at 70 °S is also provided in parentheses for both the atmosphere and ocean members and one model has 40 members; these members were all run with the same external forcing but using different initializations that are detailed in the references mentioned in Table 1. Note that we only keep the 50 CESM2 members using the CMIP6 biomass burning protocol, and the other 50 members (smoothed biomass burning) were excluded from our analysis, to allow for a fair comparison with other models. These models are the same as the ones used in a previous Arctic sea-ice study (Docquier et al. 2024b), except that only 30 ensemble members were considered for MPI-ESM1.2-LR in this previous study due to data availability at that time.

Both EC-Earth3 and CanESM5 use the same ocean and sea-ice model components, although EC-Earth3 uses a more recent version of these components. All other models present different atmosphere and ocean models. The nominal atmospheric resolution varies between 0.7° (EC-Earth3; 30 km at 70°S) and 2.8° (CanESM5; 110 km at 70°S), while the nominal ocean resolution is 1° for all models (40 km at 70°S), except MPI-ESM1.2-LR (1.5°; 50 km at 70°S). More information about the different models can be found in the references that are provided in Table 1.

From these five models, we retrieve sea-ice concentration, surface (2 m) air temperature, SST, and sea-level pressure (SLP). These four model outputs allow to compute the different variables that we consider here, i.e. sea-ice extent, mean surface air temperature, mean SST, SAM, ASL central pressure, Niño3.4 and Dipole Mode Index (DMI).

Antarctic sea-ice extent is computed as the areal sum of all ocean grid points south of 50°S that have at least 15% sea-ice concentration. Antarctic mean surface air temperature and Antarctic mean SST are spatially averaged south of 60°S. For surface air temperature, we only compute the spatial average over ocean grid points. We also compute sea-ice extent, mean surface air temperature and mean SST for each of the five Antarctic sectors used here (Fig. 1).

SAM is computed as the difference in normalized zonal mean SLP between 40°S and 65°S (Gong and Wang 1999; Marshall 2003). For the normalization, we use the period 1971–2000 to be consistent with observations (Marshall 2003). The ASL central SLP is taken at the ASL location derived from a minima finding algorithm within the ASL sector (60°S–80°S, 170°E–298°E; Hosking et al. 2016).

We also compute the Niño3.4 index, which tracks the oceanic part of ENSO based on SST anomalies averaged over the eastern tropical Pacific (5°S–5°N, 170°W–120° W). The DMI, characterizing the IOD, is computed as the difference in SST anomalies between the average over the western equatorial Indian Ocean (10°S–10°N, 50°E–70° E) and the average over the southeastern equatorial Indian Ocean (10°S–0°, 90°E–110°E). SST anomalies for both Niño3.4 and DMI are relative to the 1991–2020 base period to be consistent with observations (Sect. 2.3).

In our analysis, summer sea-ice extent is our target variable, and we compute the seasonal mean from December to February (DJF), starting in December 1970–February 1971 and ending in December 2099–February 2100 (total of 130 data points). All other variables (previous sea-ice extent, mean surface air temperature, mean SST, SAM, ASL, Niño3.4 and DMI) are our drivers and are chosen based on previous literature (Sect. 1). For the drivers, we compute the seasonal means over the previous spring season (October-December, OND), starting in 1970 and ending in 2099 (130 data points). We choose to focus on the spring season as previous studies also show the importance of spring atmospheric conditions on the summer Antarctic sea-ice minima (e.g. Mezzina et al. 2024b). However, we also present some results with the previous winter season (July–August, JAS) at the pan-Antarctic scale for completeness. We find that using SON (September-November) instead of OND for the drivers leads to weaker causal influences, but it does not affect the main results of our study (Fig. A1). Additionally, by using OND instead of SON in our study, we better take the atmospheric influence into account, which usually operates at shorter time scales. Also, even if there is one month overlap between OND and DJF, the OND seasonal mean leads the DJF seasonal mean by two months, so such a framework allows to check the two-month lag influence.

We do not consider the IPO due to its large correlation with Niño3.4 ($R \geq 0.94$ for all models), resulting in redundant results in terms of causal influences. We take SST instead of subsurface ocean temperature (100–200 m depth; Purich and Doddridge 2023), as the former provides larger values of causal influence on summer sea-ice extent. We have also made an additional test with one of the models (ACCESS-ESM1.5) involving both the mean meridional wind stress around 60°S and the mean mixed layer depth poleward of 60°S in each Antarctic sector. We found a relatively limited direct influence of wind stress in the Weddell Sea ($\tau = 2\%$) and Ross Sea ($\tau = 1\%$), and a very weak influence of mixed layer depth in the Indian Ocean ($\tau < 1\%$). Thus, we do not consider these variables in our main analysis.

As the causal method used here assumes stationarity, we remove the trend in all variables by removing the ensemble mean from each different member, in a similar way as in Docquier et al. (2024b). Finally, before computing the rate of information transfer and the correlation, we concatenate all members of the same model in a single time series for each variable, which brings between 5200 and 6500 data points for each model and thus increases the statistical significance of our results. Correlation values are similar regardless of computing them over the concatenated time series or over each member separately and then averaging them (Fig. A2).

2.3 Reference products

We use monthly mean data from both satellite observations and reanalyses as reference products. For sea-ice extent, we retrieve the sea-ice index (OSI-420, version 2.2) from the European Organisation for the Exploitation of Meteorological Satellites (EUMETSAT) Ocean and Sea Ice Satellite Application Facility (OSI SAF 2023) from 1979 to 2023 (January and February 2024 are also taken to compute summer sea-ice extent). This product is computed from the 25 km resolution OSI SAF sea-ice concentration product (Lavergne et al. 2019). Sea-ice extent is available for both the pan-Antarctic scale and the different Antarctic sectors as defined here. The ECMWF Reanalysis v5 (ERA5; Hersbach et al. 2020) on a 0.25° grid is used for computing the mean surface air temperature as the spatial average south of 60° S (for pan-Antarctic scale and different Antarctic sectors; only over ocean grid points) from 1982 to 2023. We retrieve SST from the Operational Sea Surface Temperature and Sea Ice Analysis (OSTIA) dataset (0.05° resolution) from 1982 to 2023 (Good et al. 2020) and compute the spatial average south of 60°S for both the pan-Antarctic scale and the different Antarctic sectors. The SAM index is based on SLP observations at 12 different stations, and we use data from 1970 to 2023 (Marshall 2003). We use ASL central pressure data, derived from ERA5 reanalysis, from 1970 to 2023 (Hosking et al. 2016). Niño3.4 and DMI observations are based on the NOAA Extended Reconstruction SSTs Version 5 (ERSSTv5; SST anomalies relative to the 1991–2020 base period), and we collect data from 1970 to 2023.

To compute the rate of information transfer on observed and reanalysis products, we use the 1982–2023 period that overlaps all datasets. For our target variable (summer sea-ice extent), we take December 1982–February 1983 as a first data point, and December 2023–February 2024 as a last data point (total of 42 data points). For our drivers, we compute seasonal means over the previous spring season (OND) from 1982 to 2023 (42 data points). Similarly to the models (Sect. 2.2), we also make an additional test with the previous winter (JAS) season at the pan-Antarctic scale only. Since we only have one member for our reference products, we remove the linear trend from all variables before applying our causal method.

2.4 Liang-Kleeman information flow

Based on the first principles of information theory, Liang (2014) derived a maximum-likelihood estimator of the rate of information transfer from one time series (which we call the 'driver') to another time series (which we name the 'target'), under a linear assumption. The approach has been successfully validated for some nonlinear synthetic problems (Liang 2014, 2021) and can reproduce key causal influences in the real world (e.g. Liang 2014; Hagan et al. 2022; Docquier et al. 2024b; Vannitsem et al. 2025).

In our study, the rate of information transfer from variable x_j (driver) to variable x_i (target), noted $T_{j\to i}$, is computed in a multivariate framework via Liang (2021):

$$T_{j\to i} = \frac{1}{\det\,\mathrm{C}} \cdot \sum_{k=1}^{d} \Delta_{jk} C_{k,di} \cdot \frac{C_{ij}}{C_{ii}}, \tag{1}$$

where $\mathbf{C}$ is the covariance matrix, d is the number of variables, Δ_{jk} are the cofactors of $\mathbf{C}$ ($\Delta_{jk} = (-1)^{j+k} M_{jk}$, where M_{jk} are the minors), $C_{k,di}$ is the sample covariance between all x_k and the Euler forward difference approximation of $\mathrm{d}x_i/\mathrm{d}t$, C_{ij} is the sample covariance between x_i and x_j, and C_{ii} is the sample variance of x_i. In this context, the rate of information transfer $T_{j\to i}$ represents the direct causal influence of x_j on x_i, taking into account the influence of other variables considered in the system on x_i (including the self-influence). Equation (1) shows that T only depends on the terms of the covariance matrix $\mathbf{C}$ as well as the covariance between all drivers and the temporal derivative of the target variable, which makes the calculation relatively easy. If the covariance (or correlation R) between x_i and x_j is zero, then T in the two directions is also zero; however, $R \neq 0$ does not imply that $T \neq 0$.

To be able to compare causal influences between each other, we normalize the rate of information transfer as in Liang (2021) and express it in percent:

$$\tau_{j\to i} = \frac{T_{j\to i}}{Z_i}, \tag{2}$$

where Z_i is the normalizer, computed as follows:

$$Z_i = \sum_{k=1}^{d} |T_{k\to i}| + \left| \frac{dH_i^{noise}}{dt} \right|, \tag{3}$$

where the first term on the right-hand side represents the information flowing from all variables x_k to the target variable x_i (including the influence of x_i on itself), and the last term is the effect of noise (taking stochastic effects into account). When $\tau_{j\to i}$ is significantly different from 0, x_j has an influence on x_i, while if $\tau_{j\to i} = 0$ there is no influence. In our study, we only use the absolute value of τ, which indicates the strength of the causal influence.

Statistical significance of $\tau_{j\rightarrow i}$ is computed via bootstrap resampling with replacement of all terms included in equations (1)-(3), with 1000 bootstrap realizations, and using a significance level α = 1%. The rate of information transfer τ is computed for each bootstrap realization, and the error in τ, which we refer to as ϵ_τ, is calculated as the standard deviation across all τ bootstrapped values. If the confidence interval $\tau \pm 2.57\,\epsilon_\tau$ does not contain the zero value, then τ is significant at the 1% level; otherwise, it is not significant.

We compute the rate of information transfer $|\tau|$ (absolute value) for all pairs of variables at the pan-Antarctic scale and for each different Antarctic sector (over the period 1970–2100 for all five models and 1982–2023 for observations). In order to check which spurious links are removed from the causal analysis, we also compute the Pearson correlation coefficient R over the same period as the rate of information transfer. The statistical significance associated with the correlation is computed in a similar way as the rate of information transfer to ensure consistency (bootstrap resampling with replacement using 1000 realizations). Note that SAM, ASL, Niño3.4 and DMI are identical for all sectors, while summer and previous sea-ice extent, mean surface air temperature and mean SST vary by sector.

To present the results from our causal analysis, we produce plots of the rate of information transfer from the different drivers to summer sea-ice extent (Figs. 3a, 5a, 7), which we compare to corresponding correlation coefficients (Figs. 3b, 5b, A8). We also show causal graphs representing the full network of interactions, with nodes representing the different variables (drivers and target) and directed edges showing the causal links (Figs. 4, 8, 9, 10).

In the causal graphs, only statistically significant causal influences (α = 1%) with a rate of information transfer $|\tau|$ larger than 1% are shown, and we only display causal influences that participate directly or indirectly in changing summer sea-ice extent. Thus, for example, if there is a causal influence between Niño3.4 and DMI, but none of these two variables has an effect (direct or indirect) on summer sea-ice extent, this influence is not displayed in the causal graph. To summarize results of the causal graphs, we compute the degree of centrality for each node (variable) as the sum of incoming and outgoing causal edges, following the methodology of Tyrovolas et al. (2023). The variable with the largest degree of centrality is displayed in brackets after the panel title of each causal graph. Causal graphs are not produced for observations as the number of statistically significant causal influences is very low due to the shortness of time series.

In order to check the temporal evolution of causal influences, we also compute $|\tau|$ for each range of 10 years separately across all members of the same model, meaning that we have between 400 and 500 data points for each 10-year period depending on the model. No detrending is performed in this case as the time periods are relatively short. Statistical significance is computed in the same way as the boostrap method described above (1000 bootstrap realizations and α = 1%) for each 10-year period. Due to the availability of only one realization in observations and reanalyses, we do not compute the observed rate of information transfer for those 10-year periods, as the number of data points is too small.

3 Results

3.1 Pan-Antarctic scale

Time series of the different variables considered in this study at the pan-Antarctic scale are presented in Fig. 2. CanESM5 displays the largest summer (DJF) and spring (OND) sea-ice extent throughout the whole model simulation (Fig. 2a, b), associated with the coldest surface air temperature and SST (Fig. 2c, d). By contrast, EC-Earth3 and MPI-ESM1.2-LR have the lowest sea-ice extent, both in summer and spring (Fig. 2a, b), and EC-Earth3 is the warmest model (Fig. 2c, d). ACCESS-ESM1.5 and CESM2 present values of sea-ice extent, surface air temperature and SST in between the extreme values of CanESM5 and EC-Earth3, and show the best agreement with satellite observations of sea-ice extent (Fig. 2a, b).

Looking at the ensemble mean, all models show a negative trend in sea-ice extent over the observational period and cannot reproduce the positive observed trend between 1979 and 2015 (Fig. 2a, b). However, Roach et al. (2020) caution that this model bias should not be used as a criterion to exclude them from climate projections, as the role of internal variability in driving the observed trend has potentially been large. The ensemble means of all models show a positive trend in SAM, a negative trend in ASL and a positive trend in Niño3.4, in agreement with observations (Fig. 2e–g). The model member spreads of SAM, ASL, Niño3.4 and DMI include observational values of these indices (Fig. 2e–h).

At the pan-Antarctic scale, the largest driver of changes in summer sea-ice extent at interannual time scale over 1970–2100, according to the Liang-Kleeman information flow, is the previous spring sea-ice extent for all models, except CanESM5, for which the mean spring SST is more important (Fig. 3a). This is in agreement with observations, although the results are not statistically significant due to the short observational period (42 years). Mean spring SST and surface air temperature are also important drivers for three models (CanESM5, MPI-ESM1.2-LR and EC-Earth3) and two models (MPI-ESM1.2-LR and CanESM5), respectively. Additionally, SAM plays a role for four models (all

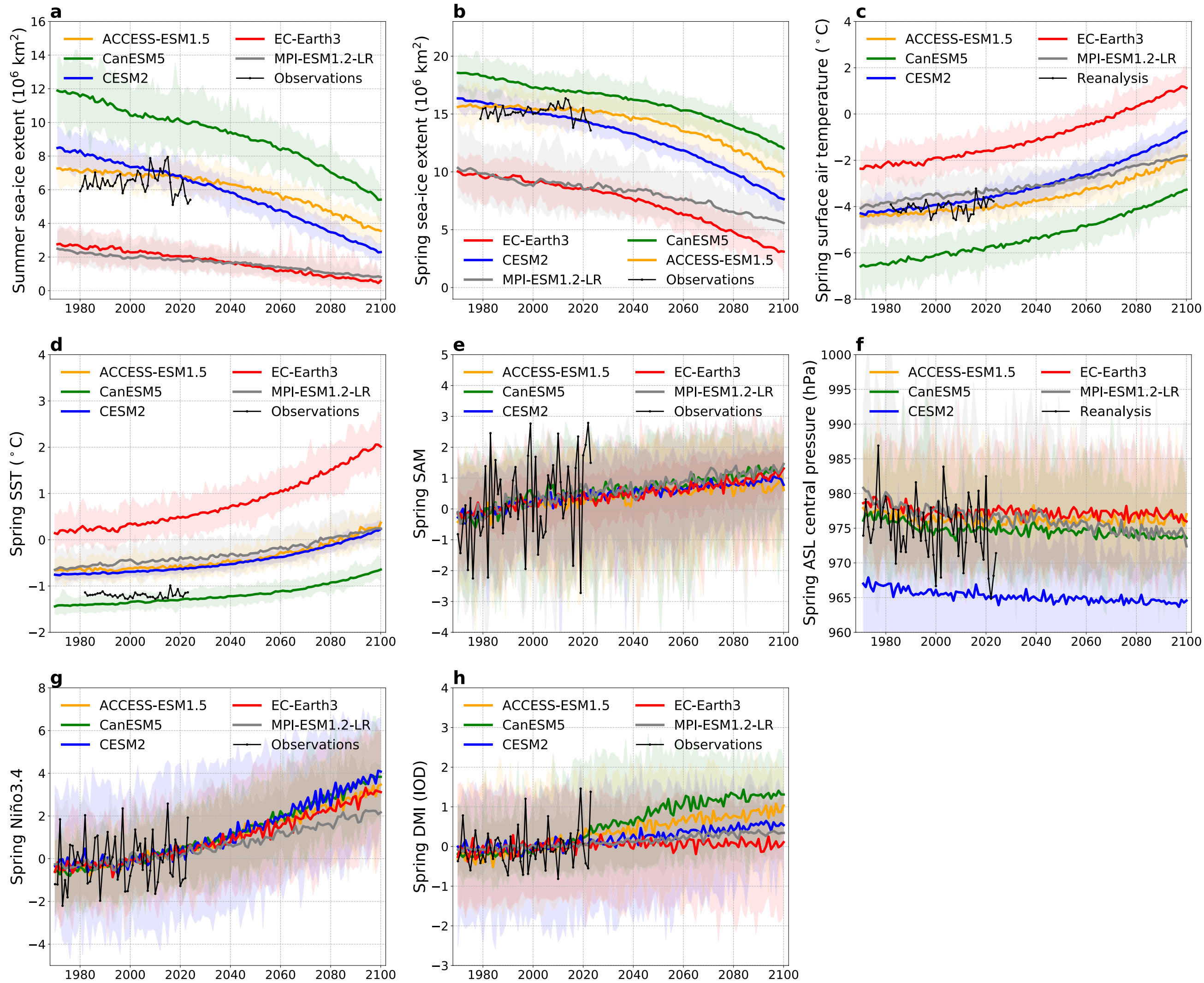

Fig. 2 Time series of the different variables for the five large ensembles using CMIP6 historical (1970–2014) and SSP3−7.0 (2015–2100) simulations. Solid colored curves represent ensemble means and shading shows the ensemble spread (between minimum and maximum). Black solid lines represent observations and reanalyses. **a** Summer (DJF) Antarctic sea-ice extent. **b** Spring (OND) Antarctic sea-ice extent. **c** Spring (OND) Antarctic surface air temperature. **d** Spring (OND) Antarctic sea-surface temperature (SST). **e** Spring (OND) Southern Annular Mode (SAM). **f** Spring (OND) Amundsen Sea Low (ASL) central pressure. **g** Spring (OND) Niño3.4. **h** Spring (OND) Dipole Mode Index (DMI)

models except MPI-ESM1.2-LR), even if the values of information transfer are comparatively low ($|\tau| < 5\%$). All five models and observations present statistically significant correlations between summer sea-ice extent on the one hand and previous spring sea-ice extent, surface air temperature and SST on the other hand (Fig. 3b). This suggests that results based solely on correlations should be interpreted with caution. For models, this indicates that the negative correlations between surface air temperature and summer sea-ice extent on the one hand, and between SST and summer sea-ice extent on the other hand (Fig. 3b) are not necessarily linked to direct causal influences from temperature to sea-ice extent (Fig. 3a).

The full network of causal interactions (discarding low values of information transfer, i.e. $|\tau| < 1\%$) reveals that the situation is more complex than simply looking at direct drivers and that each model has its particular features (Fig. 4). For example, SST plays a key role in CanESM5, as it is influenced by five other variables (spring sea-ice extent, surface air temperature, SAM, Niño3.4 and DMI; Fig. 4b), which could partly explain why the rate of information transfer from SST to summer sea-ice extent is large for this model compared to other models (Fig. 3a). For ACCESS-ESM1.5, although there is no direct connection from SST to summer sea-ice extent, an indirect pathway via spring sea-ice extent can be identified (Fig. 4a). We can also see that surface air temperature is somewhat isolated from other variables and

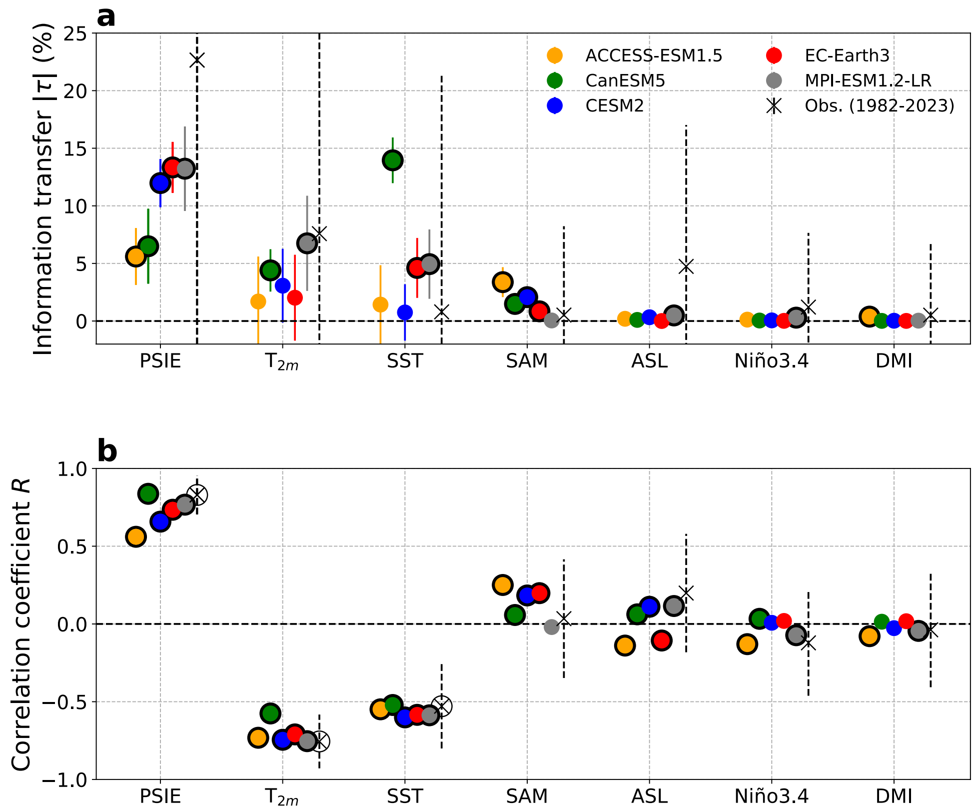

Fig. 3 **a** Rate of information transfer (absolute value) from previous (OND) sea-ice extent (PSIE), surface air temperature (T_{2m}), sea-surface temperature (SST), Southern Annular Mode (SAM), Amundsen Sea Low (ASL), Niño3.4, and Dipole Mode Index (DMI) to summer (DJF) sea-ice extent at the pan-Antarctic scale over 1970–2100. **b** Corresponding correlation coefficients. Colored circles represent the five large ensembles, with significant values at the 1% level highlighted by black contours and the corresponding error bars. Crosses show observations/reanalyses, with significant values at the 1% level highlighted by black circles (error bars are represented by dashed vertical lines)

does not show any statistically significant causal connection with the rest of the variables for both ACCESS-ESM1.5 (Fig. 4a) and CESM2 (Fig. 4c). EC-Earth3 does not display any direct causal influence from surface air temperature to summer sea-ice extent, but rather shows an indirect pathway from the former to the latter via spring sea-ice extent (Fig. 4d). Additionally, while SAM has a direct influence on summer sea-ice extent for three models (ACCESS-ESM1.5, CanESM5 and CESM2), it also causes indirect changes in summer sea-ice extent via SST for the two other models (EC-Earth3 and MPI-ESM1.2-LR).

If we take the previous winter (JAS) mean for our different drivers instead of the previous spring mean, we find that causal influences generally become weaker, especially for the previous sea-ice extent, which is now statistically significant only for three models (Fig. 5a). The SST influence is still present for three models, but with lower rate of information transfer for CanESM5 and EC-Earth3, and a larger value for CESM2. For surface air temperature, the situation reverses, with the two models showing a causal influence in spring (MPI-ESM1.2-LR and CanESM5) not displaying any influence in winter, while the three other models now show a significant information transfer. This is particularly marked for EC-Earth3, which shows a large value of information transfer in winter ($|\tau| = 17\%$; Fig. 5a), while this is not the case in spring (Fig. 3a). The role of SAM almost completely disappears in winter compared to spring, and other climate indices (ASL, Niño3.4 and DMI) still have very weak values of information transfer. The network of causal connections is less dense in winter (Fig. A3) compared to spring (Fig. 4). These results suggest that taking the few months just before the summer season provides larger causal influences than about 6 months before.

We acknowledge that causal influences of the different potential drivers of summer Antarctic sea-ice extent may change over time. That is why we conduct an additional analysis in which we compute the rate of information transfer across all members of the same model for each 10-year period. We find that the influence of the previous spring sea-ice extent on summer sea-ice extent is generally the largest and statistically significant between 1980 and 2050 for EC-Earth3, MPI-ESM1.2-LR and CESM2 (Fig. 6a). Only CESM2 and CanESM5 show statistically significant causal influences after 2050 (in 2080–2090). EC-Earth3 presents a negative trend in the causal influence of previous sea-ice extent (Fig. 6a). For the influence of surface air temperature, only CanESM5 shows a statistically significant rate of information transfer during the last part of the period (2060–2090), which leads to a positive trend for this model (Fig. 6b). On the contrary, the influence of surface air temperature from EC-Earth3 decreases over time, despite the absence of statistically significant influences in any 10-year time period. The SST influence increases over time for both CanESM5 and CESM2, with the former model displaying

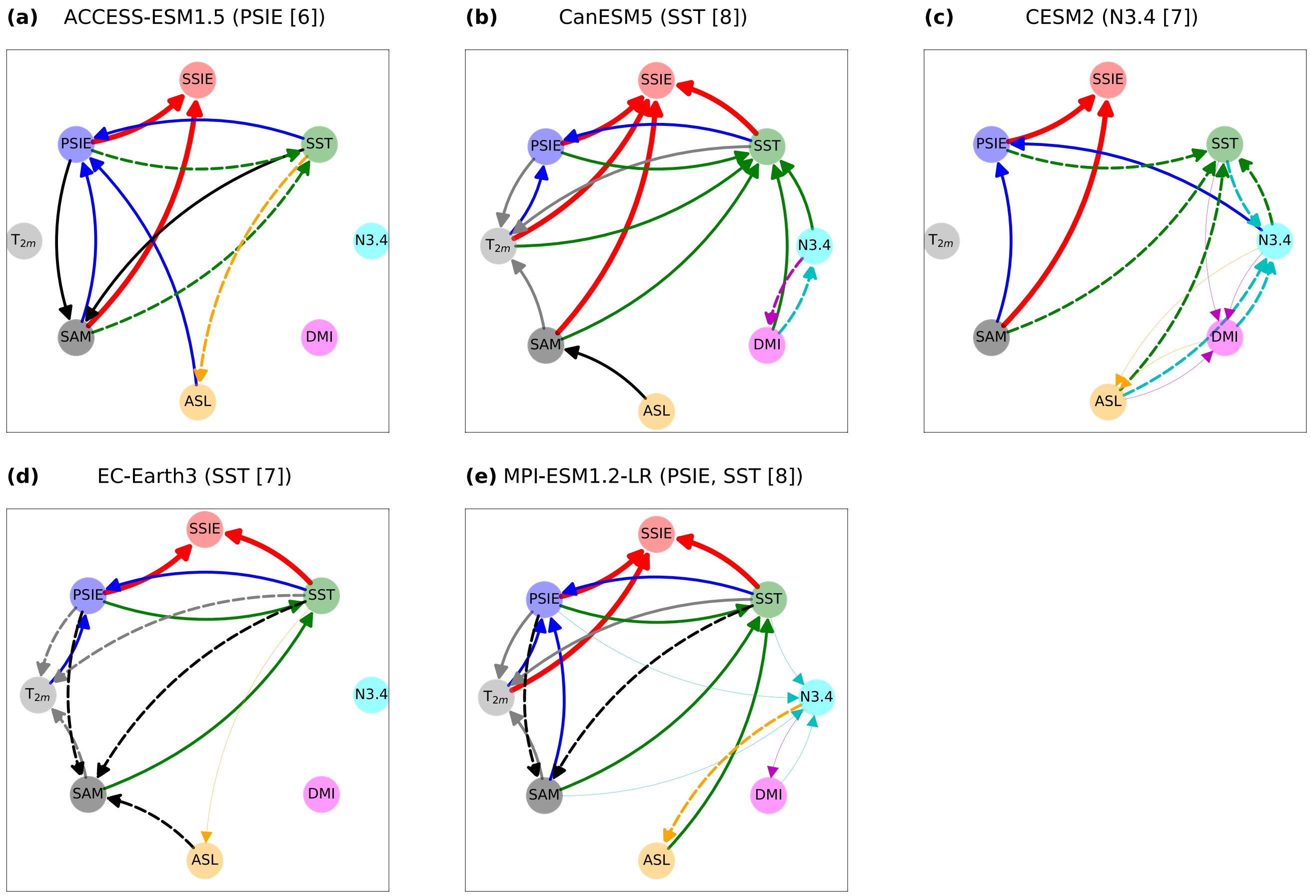

Fig. 4 Causal graphs showing statistically significant (1% level) causal influences between all variables at the pan-Antarctic scale for the five large ensembles: **a** ACCESS-ESM1.5, **b** CanESM5, **c** CESM2, **d** EC-Earth3, and **e** MPI-ESM1.2-LR. All variables except summer sea-ice extent (SSIE) are averaged over spring (OND). The color of each arrow matches the influenced node: red for summer sea-ice extent (SSIE), blue for previous sea-ice extent (PSIE), gray for surface air temperature (T_{2m}), green for sea-surface temperature (SST), black for Southern Annular Mode (SAM), orange for Amundsen Sea Low (ASL), cyan for Niño3.4 (N3.4), and magenta for Dipole Mode Index (DMI). The arrow thickness and style indicates the proximity to SSIE in the causal chain: thick solid arrows for direct links to SSIE, moderately thick solid arrows for indirect links, moderately thick dashed arrows for second-indirect links, thin solid arrows for third- and fourth-indirect links. The variables in brackets after each panel title represent the nodes with the largest degree of centrality for each model (with the respective value in squared brackets)

statistically significant causal influences during the whole twenty-first century (Fig. 6c). SST also has some influence for EC-Earth3 in the first half of the period (1980–2000 and 2010–2020). Despite a statistically significant causal influence of SAM for ACCESS-ESM1.5, CESM2 and CanESM5 during some 10-year periods, values of information transfer remain low over the whole period ($|\tau| < 5\%$; Fig. 6d). Thus, the positive trend in SAM (Fig. 2e) does not lead to an increase in its influence on summer sea-ice extent.

In summary, the causal analysis at the pan-Antarctic scale shows that some patterns are recurrent among models, e.g. the relatively large influence (whether direct or indirect) of proximate drivers, such as spring sea-ice extent (largest and most robust influence among the different models), SST and surface air temperature on summer sea-ice extent, while teleconnection patterns (Niño3.4 and DMI) play a much smaller role (Fig. 4). Additionally, we find a general decrease in the previous sea-ice extent influence over time, together with an increasing SST impact along the years (Fig. 6). This interesting behavior suggests that the control of the ocean on summer sea-ice extent may be stronger in the future.

3.2 Antarctic sectors

We now turn to the causal analysis by sector, as defined in Fig. 1, to establish a potential result dependence on the region choice. We strongly suspect such a dependence due to the relatively large spatial heterogeneity in Antarctic sea-ice variability since 1979 (Raphael and Hobbs 2014), despite an apparent decrease in this spatial heterogeneity over the past decade (Schroeter et al. 2023). As previously explained in Sect. 2.4, time series of SAM, ASL, Niño3.4 and DMI remain the same as for the pan-Antarctic scale (Fig. 2e-h).

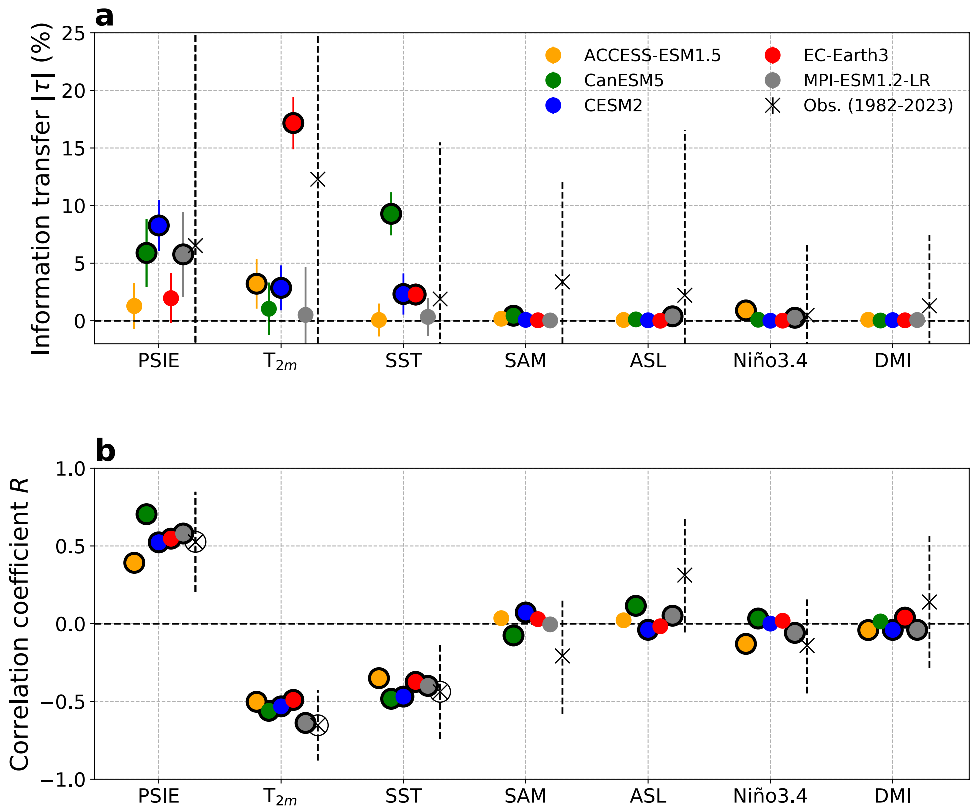

Fig. 5 **a** Rate of information transfer (absolute value) from previous winter (JAS) sea-ice extent (PSIE), surface air temperature (T_{2m}), sea-surface temperature (SST), Southern Annular Mode (SAM), Amundsen Sea Low (ASL), Niño3.4, and Dipole Mode Index (DMI) to summer (DJF) sea-ice extent at the pan-Antarctic scale over 1970–2100. **b** Corresponding correlation coefficients. Colored circles represent the five large ensembles, with significant values at the 1% level highlighted by black contours and the corresponding error bars. Crosses show observations/reanalyses, with significant values at the 1% level highlighted by black circles (error bars are represented by dashed vertical lines)

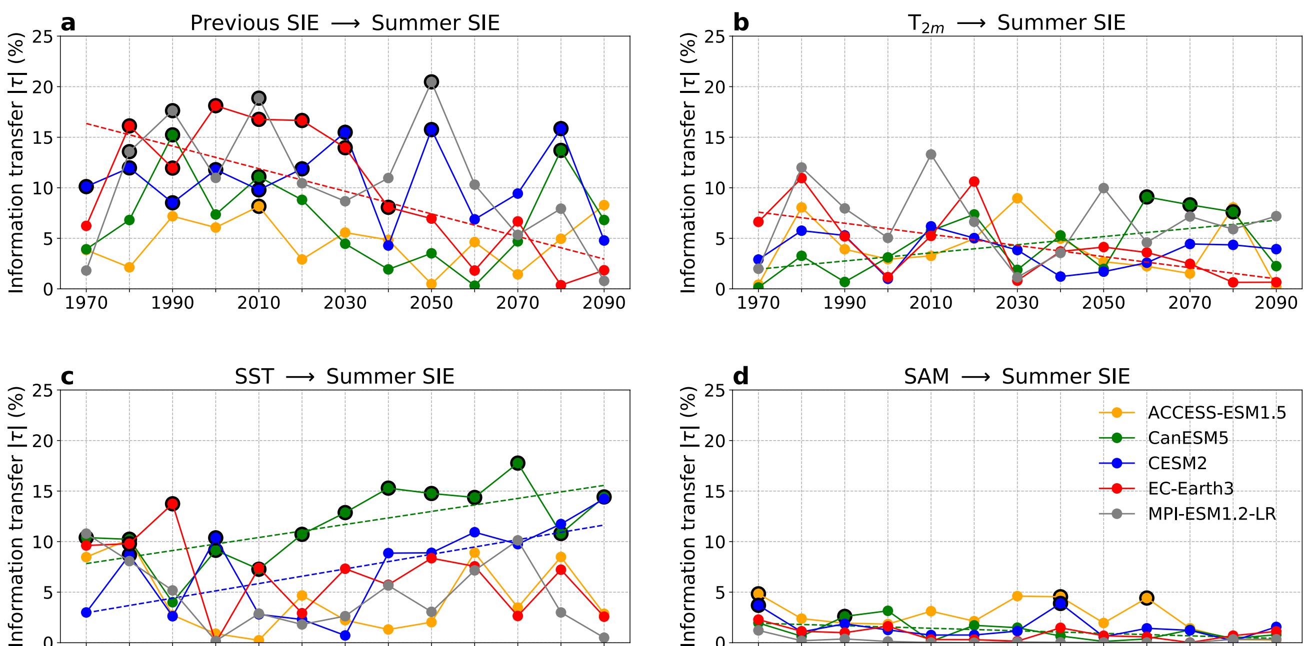

Fig. 6 Temporal evolution of the rate of information transfer (absolute value) from **a** previous (OND) sea-ice extent (SIE), **b** surface air temperature (T_{2m}), **c** sea-surface temperature (SST), and **d** Southern Annular Mode (SAM) to summer sea-ice extent at the pan-Antarctic scale for each period of 10 years over 1970–2100 (the starting year is indicated on the x-axis). Colored circles represent the five large ensembles, with significant values at the 1% level highlighted by black contours. Straight dotted lines represent the linear regressions for each model and are shown only when the slopes are statistically significant at the 10% level

Time series of summer and spring sea-ice extent, surface air temperature and SST for the different sectors are provided in the Appendix (Figs. A4–A7). Similarly to the pan-Antarctic scale, CanESM5 is generally colder and has more sea ice in all Antarctic sectors, and EC-Earth3 is generally warmer and has less sea ice. Below, we first present an analysis of the direct drivers of summer sea-ice extent (Sect. 3.2.1). We then build causal graphs representing the full network of causal interactions for three different models: one moderate (neither warm nor cold) model (ACCESS-ESM1.5), one cold model (CanESM5) and one warm model (EC-Earth3) (Sect. 3.2.2).

3.2.1 Direct drivers of summer sea-ice extent

The results from our causal analysis reveals that in the Bellingshausen-Amundsen Seas, the previous spring sea-ice extent is the largest direct driver of changes in summer sea-ice extent for all five models (Fig. 7b). However, the rates of information transfer greatly differ between models, ranging between $|\tau| = 4\%$ for EC-Earth3 and $|\tau| = 28\%$ for CanESM5. ACCESS-ESM1.5 has the value of information transfer closest to observations ($|\tau| = 9\%$), but the observed value is not statistically significant. SST and surface air temperature also influence summer sea-ice extent for three and two models, respectively. The influence of SAM is relatively limited with low values of information transfer ($|\tau| < 2\%$),

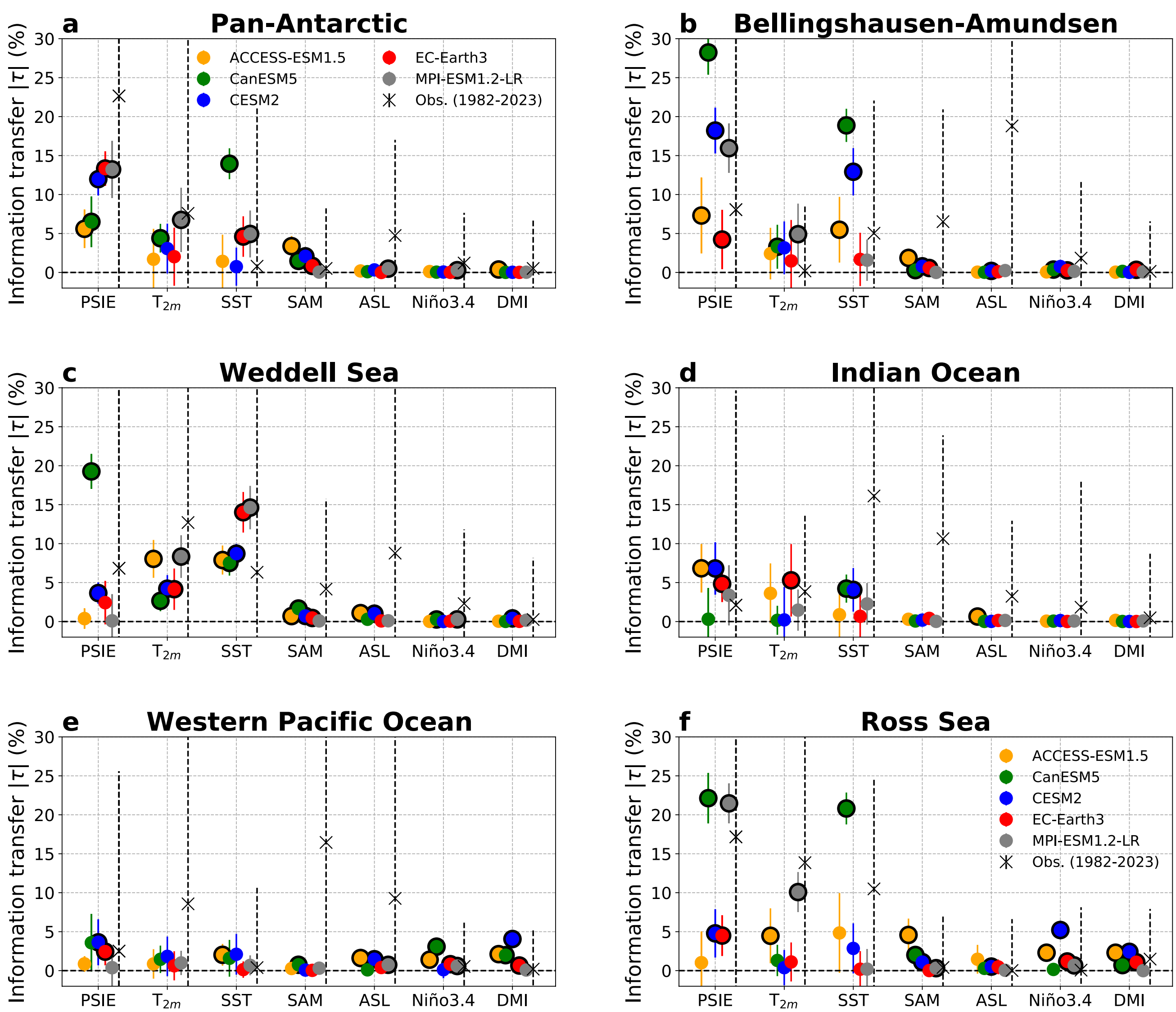

Fig. 7 Rate of information transfer (absolute value) from previous (OND) sea-ice extent (PSIE), surface air temperature (T_{2m}), sea-surface temperature (SST), Southern Annular Mode (SAM), Amundsen Sea Low (ASL), Niño3.4, and Dipole Mode Index (DMI) to summer sea-ice extent **a** at the pan-Antarctic scale and **b**–**f** in the different Antarctic sectors over 1970–2100. Colored circles represent the five large ensembles, with significant values at the 1% level highlighted by black contours and the corresponding error bars. Crosses show observations/reanalyses, with significant values at the 1% level highlighted by black circles (error bars are represented by dashed vertical lines)

and other climate indices (ASL, Niño3.4 and DMI) display almost no influence for the models considered here.

The Weddell Sea presents a dominant role of SST for all models ($7.5 < |\tau| < 15\%$). Surface air temperature also has an important influence for all models ($2.5 < |\tau| < 8\%$; Fig. 7c). Observations display a large but not significant causal influence of surface air temperature on summer sea-ice extent.

Compared to the Bellingshausen-Amundsen and Weddell Seas, rates of information transfer are lower in the Indian Ocean (Fig. 7d). Three models (ACCESS-ESM1.5, CESM2 and EC-Earth3) display an influence of spring sea-ice extent, two models (CanESM5 and CESM2) show an effect of SST, and one model (EC-Earth3) has an influence of surface air temperature, while MPI-ESM1.2-LR does not present any influence of any of the drivers considered here on summer sea-ice extent. It is interesting to note that no causal influence appears in observations, while five pairs of observed correlations (summer sea-ice extent with previous sea-ice extent, surface air temperature, SST, SAM and Niño3.4) are statistically significant (Fig. A8d).

Like for the Indian Ocean, rates of information transfer in the Western Pacific Ocean are also low ($|\tau| < 5\%$) for all five models (Fig. 7e). On the contrary, and interestingly,

Table 2 Main drivers of summer sea-ice extent for each model (columns) and each sector (rows)

	ACCESS-ESM1.5	**CanESM5**	**CESM2**	**EC-Earth3**	**MPI-ESM1.2-LR**
Pan-Antarctic	PSIE / PSIE	**SST / SST**	**PSIE** / **N3.4**	**PSIE** / **SST**	**PSIE** / **PSIE**, **SST**
Bell.-Amundsen Seas	PSIE / SST	**PSIE** / SST	**PSIE** / PSIE, SST, N3.4	PSIE / **PSIE**, **SST**	**PSIE** / PSIE, SST, T_{2m}
Weddell Sea	T_{2m} / SST	**PSIE** / PSIE, SST	SST / **SST**	**SST** / SST	**SST** / **SST**
Indian Ocean	PSIE / PSIE	SST / SST	PSIE / SST	T_{2m} / T_{2m}	- / -
Western Pacific Ocean	SST / SST	N3.4 / N3.4, DMI	DMI / **DMI**	PSIE / T_{2m}, SST	- / -
Ross Sea	SAM / **N3.4**	**PSIE** / **PSIE**	N3.4 / **PSIE**	PSIE / **DMI**	**PSIE** / SST, N3.4

In each table entry, the variable on the left of the slash sign is the direct driver with the largest absolute rate of information transfer $|\tau|$ (absence of direct driver if $|\tau| < 1\%$; Sect. 3.2.1), and the variable(s) on the right of the slash sign is (are) the driver(s) with the largest degree of centrality (Sect. 3.2.2). We highlight in bold font direct drivers with $|\tau| > 10\%$ (left of the slash sign) and drivers with a degree of centrality equal or larger than 7, i.e. at least 7 incoming and outgoing edges (right of the slash sign). PSIE: previous sea-ice extent, T_{2m}: surface air temperature, SST: sea-surface temperature, SAM: Southern Annular Mode, ASL: Amundsen Sea Low, N3.4: Niño3.4, DMI: Dipole Mode Index

the observed influence of SAM is large ($|\tau| = 18\%$) but not statistically significant at the 1% level. Despite these low values for models, Niño3.4 and DMI also have an effect on summer sea-ice extent for four models (Fig. 7e), which makes sense due to the relative proximity of the eastern Central Pacific and Indian Ocean to the Western Pacific Ocean sector.

The Ross Sea is characterized by very large influences of spring sea-ice extent in CanESM5 and MPI-ESM1.2-LR ($|\tau| > 20\%$), SST in CanESM5 ($|\tau| = 21\%$), and surface air temperature in MPI-ESM1.2-LR ($|\tau| > 10\%$) (Fig. 7f). SAM, Niño3.4 and DMI also display some direct influence on summer sea-ice extent for a majority of models, but with weaker values of information transfer (Fig. 7f).

Overall, this analysis shows that the main direct drivers of changes in summer sea-ice extent are mainly proximate in most sectors (except in the Western Pacific Ocean) and for most models, with a few differences on the exact driver between regions: previous sea-ice extent in the Bellingshausen-Amundsen Seas (Fig. 7b), SST in the Weddell Sea (Fig. 7c), a mix of previous sea-ice extent, surface air temperature and SST in the Indian Ocean (Fig. 7d), and previous sea-ice extent in the Ross Sea (Fig. 7f). This finding agrees with the results at the pan-Antarctic scale, for which proximate drivers are also predominant (Fig. 7a). On the contrary, in the Western Pacific Ocean, where rates of information transfer are considerably lower than other regions and relatively comparable from one driver to the other, we find a larger influence of remote climate indices (Niño3.4 and DMI) (Fig. 7e), compared to other sectors. This teleconnection pattern also appears in the Ross Sea (Fig. 7f). A summary of the main direct driver for each model and each sector is presented in Table 2 (left variable in each table entry).

Finally, all models present statistically significant correlations between proximate drivers (previous sea-ice extent, surface air temperature, SST) and summer sea-ice extent in all sectors (Fig. A8), while causal influences are statistically significant in only $\sim$50% of the cases (38/75; Fig. 7). This is even more marked for observations, for which 87% of the cases display statistically significant correlations for proximate drivers (Fig. A8), while none of the cases shows a statistically significant causal influence (Fig. 7). With this result, we caution against interpreting too quickly correlations as a proof of cause-effect relationships, which often proves to be wrong.

3.2.2 Causal networks

Beyond the identification of direct drivers of changes in summer sea-ice extent, it is also interesting to reconstruct the full network of causal interactions based on the

Liang-Kleeman information flow method. This way, it is also possible to analyze indirect causal links that lead to changes in summer sea-ice extent. To ease the analysis, we focus on three models that fully capture the inter-model spread: ACCESS-ESM1.5 (Fig. 8), CanESM5 (Fig. 9) and EC-Earth3 (Fig. 10). ACCESS-ESM1.5 has average values for all variables considered, with a relatively good agreement with observations, while CanESM5 is relatively cold and displays large sea-ice extent in all sectors, and EC-Earth3 is relatively warm with low sea-ice extent (Figs. A4–A7). For completeness, we also show the results of causal influences for the two remaining models in the Appendix (Figs. A9–A10). The overall importance of each driver in the causal network is computed via the degree of centrality, and the most important drivers in that respect are presented for each model and each sector in Table 2 (right variable in each table entry).

Starting with the moderately warm model (ACCESS-ESM1.5; Fig. 8), we find that SST displays the largest importance in the causal network leading to changes in summer sea-ice extent, as measured by the degree of centrality, in three out of five sectors (Bellingshausen-Amundsen Seas, Weddell Sea, and Western Pacific Ocean). In the Indian Ocean, the previous sea-ice extent plays the largest role, while in the Ross Sea, it is Niño3.4, with 7 incoming and outgoing causal edges. The Ross Sea and Western Pacific Ocean are the only sectors where ENSO (represented by Niño3.4) and IOD (represented by DMI) have some indirect and direct influence on summer sea-ice extent. The direct influence of SAM in West Antarctica (Bellingshausen-Amundsen and Ross Seas) is in agreement with previous literature (e.g. Zhang and Li 2023). For the other three sectors, SAM plays an indirect influence, via SST and previous sea-ice extent in the Weddell Sea, via previous sea-ice extent in

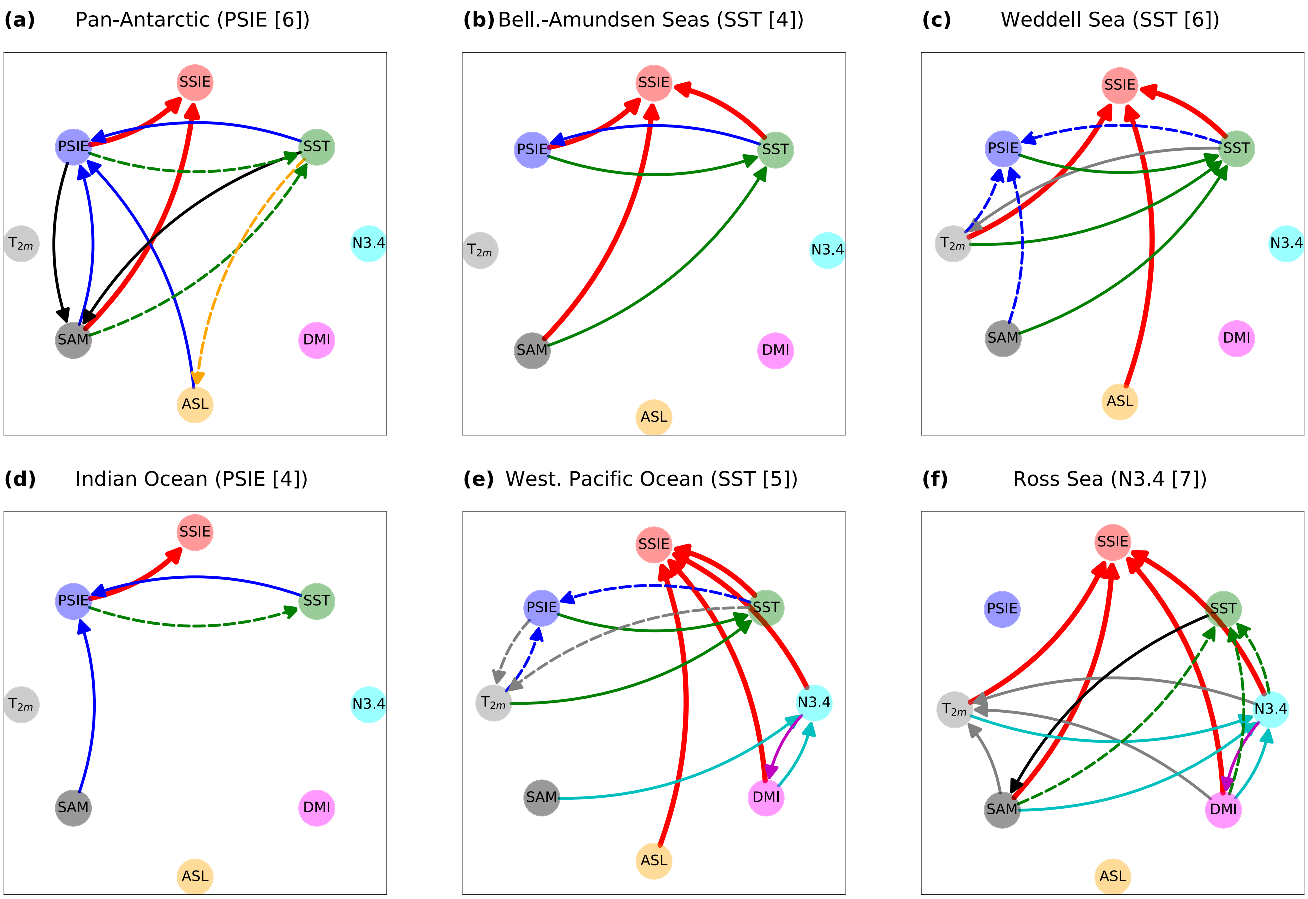

Fig. 8 Causal graphs showing statistically significant (1% level) causal influences between all variables for the ACCESS-ESM1.5 model (moderate model) **a** at the pan-Antarctic scale and in all different Antarctic sectors: **b** Bellingshausen-Amundsen Seas, **c** Weddell Sea, **d** Indian Ocean, **e** Western Pacific Ocean, **f** Ross Sea. All variables except summer sea-ice extent (SSIE) are averaged over spring (OND). The color of each arrow matches the influenced node: red for summer sea-ice extent (SSIE), blue for previous sea-ice extent (PSIE), gray for surface air temperature (T_{2m}), green for sea-surface temperature (SST), black for Southern Annular Mode (SAM), orange for Amundsen Sea Low (ASL), cyan for Niño3.4 (N3.4), and magenta for Dipole Mode Index (DMI). The arrow thickness and style indicates the proximity to SSIE in the causal chain: thick solid arrows for direct links to SSIE, moderately thick solid arrows for indirect links, moderately thick dashed arrows for second-indirect links. The variables in brackets after each panel title represent the nodes with the largest degree of centrality for each model (with the respective value in squared brackets)

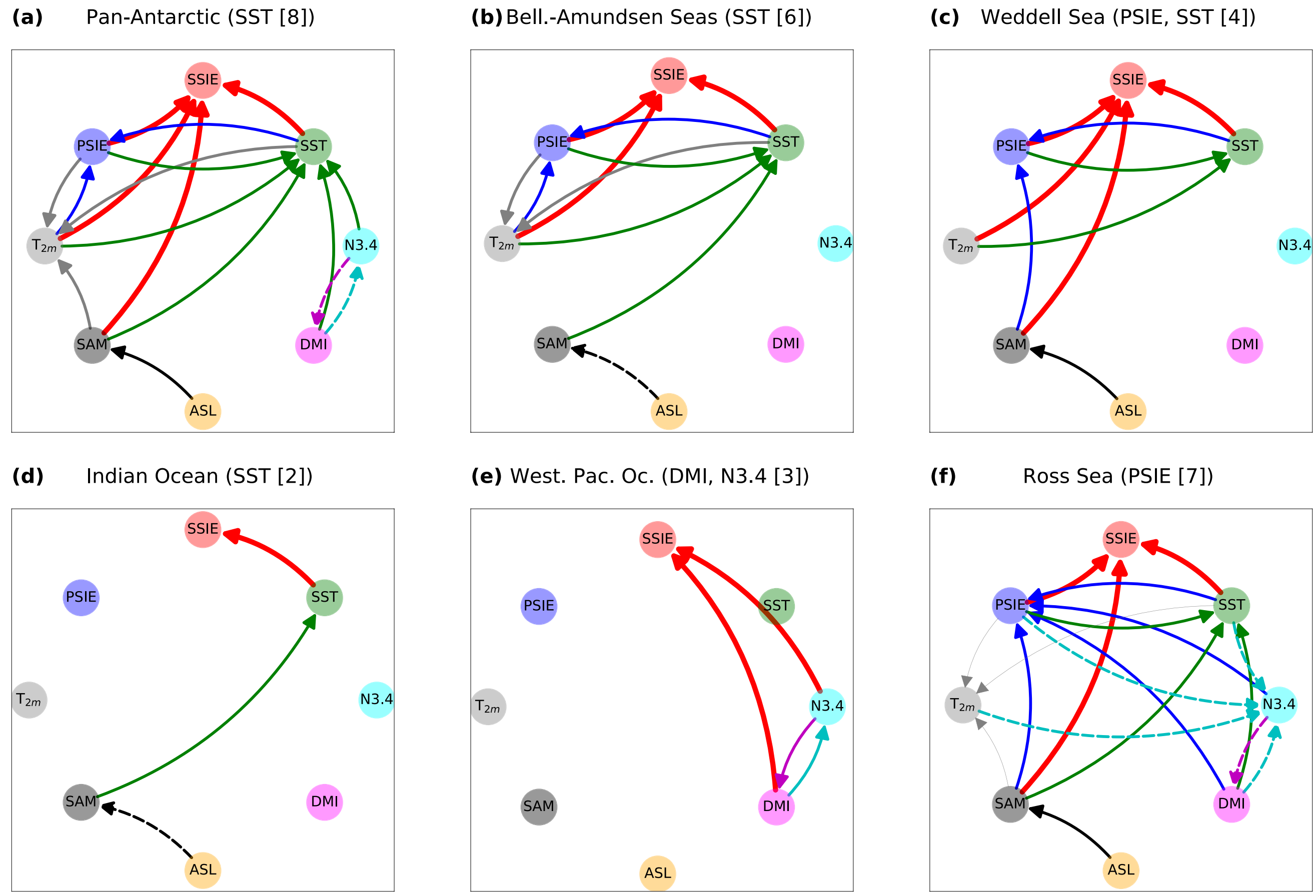

Fig. 9 Causal graphs showing statistically significant (1% level) causal influences between all variables for the CanESM5 (cold model) **a** at the pan-Antarctic scale and in all different Antarctic sectors: **b** Bellingshausen-Amundsen Seas, **c** Weddell Sea, **d** Indian Ocean, **e** Western Pacific Ocean, **f** Ross Sea. All variables except summer sea-ice extent (SSIE) are averaged over spring (OND). The color of each arrow matches the influenced node: red for summer sea-ice extent (SSIE), blue for previous sea-ice extent (PSIE), gray for surface air temperature (T_{2m}), green for sea-surface temperature (SST), black for Southern Annular Mode (SAM), orange for Amundsen Sea Low (ASL), cyan for Niño3.4 (N3.4), and magenta for Dipole Mode Index (DMI). The arrow thickness and style indicates the proximity to SSIE in the causal chain: thick solid arrows for direct links to SSIE, moderately thick solid arrows for indirect links, moderately thick dashed arrows for second-indirect links, thin solid arrows for third-indirect links. The variables in brackets after each panel title represent the nodes with the largest degree of centrality for each model (with the respective value in squared brackets)

the Indian Ocean, and via Niño3.4 in the Western Pacific Ocean. No connection appears between SAM and ASL in any sector for this model, but ASL has a direct influence on summer sea-ice extent in the Weddell Sea and Western Pacific Ocean.

When we turn to the cold model (CanESM5; Fig. 9), SST also has the largest degree of centrality in three sectors (Bellingshausen-Amundsen Seas, Weddell Sea, and Indian Ocean). In the Western Pacific Ocean, Niño3.4 and DMI have the largest importance, while in the Ross Sea the previous sea-ice extent plays the largest role. The previous sea-ice extent is also an important driver of changes in summer sea-ice extent in the Weddell Sea. Similarly to the moderate model, the Ross Sea also displays the densest network of causal interactions for the cold model, with a relatively large role of ENSO (6 incoming and outgoing causal edges). On the contrary, the Indian Ocean and Western Pacific Ocean present a very small number of statistically significant causal influences. SAM either directly influences summer sea-ice extent in the Weddell and Ross Seas, or causes indirect changes via SST in the Bellingshausen-Amundsen Seas, Indian Ocean and Ross Sea. The ASL has some influence on SAM in all sectors, except in the Western Pacific Ocean.

The warm model (EC-Earth3; Fig. 10) also highlights the large role of SST (as measured by the degree of centrality) in three sectors (Bellingshausen-Amundsen Seas, Weddell Sea and Western Pacific Ocean). The SST link to summer sea-ice extent is both direct and indirect (via surface air temperature) in the Weddell Sea, while its influence is only indirect in the Bellingshausen-Amundsen Seas and Western Pacific Ocean, mainly via the previous sea-ice extent. Surface air temperature plays a major role in the Indian Ocean and Western Pacific Ocean. In the Ross Sea, DMI displays

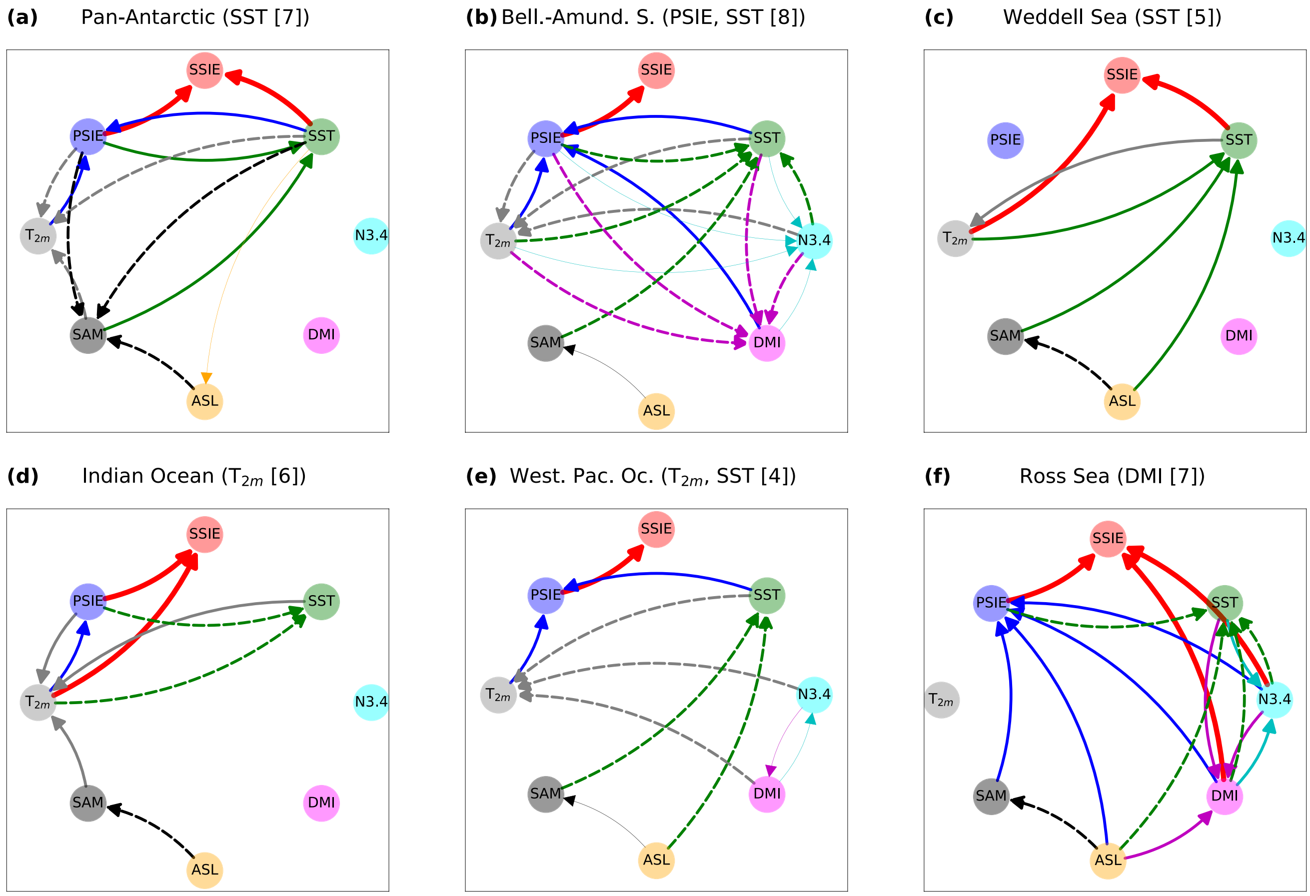

Fig. 10 Causal graphs showing statistically significant (1% level) causal influences between all variables for the EC-Earth3 model (warm model) **a** at the pan-Antarctic scale and in all different Antarctic sectors: **b** Bellingshausen-Amundsen Seas, **c** Weddell Sea, **d** Indian Ocean, **e** Western Pacific Ocean, **f** Ross Sea. All variables except summer sea-ice extent (SSIE) are averaged over spring (OND). The color of each arrow matches the influenced node: red for summer sea-ice extent (SSIE), blue for previous sea-ice extent (PSIE), gray for surface air temperature (T_{2m}), green for sea-surface temperature (SST), black for Southern Annular Mode (SAM), orange for Amundsen Sea Low (ASL), cyan for Niño3.4 (N3.4), and magenta for Dipole Mode Index (DMI). The arrow thickness and style indicates the proximity to SSIE in the causal chain: thick solid arrows for direct links to SSIE, moderately thick solid arrows for indirect links, moderately thick dashed arrows for second-indirect links, thin solid arrows for third-indirect links. The variables in brackets after each panel title represent the nodes with the largest degree of centrality for each model (with the respective value in squared brackets)

the largest degree of centrality, with 7 incoming and outgoing causal edges. The SAM influence on summer sea-ice extent is indirect in all sectors, and SAM is affected by ASL in all sectors.

To summarize, all three types of models (moderate, cold and warm models) show that SST displays the largest importance in the causal network in both the Bellingshausen-Amundsen and Weddell Seas. The Indian Ocean presents the least dense causal network for all three types of models, with a larger influence of previous sea-ice extent in the moderate model, SST in the cold model, and surface air temperature in the warm model. In the Western Pacific Ocean, SST plays a relatively large role in influencing summer sea-ice extent for both the moderate and warm models, while teleconnections (DMI and Niño3.4) are more important for the cold model. In the Ross Sea, the role of ENSO and IOD is generally important for all three types of models. Although SAM is never the largest actor in any region for any model, it displays an influence on summer sea-ice extent (mainly indirectly via SST) for the three models, and is influenced by ASL in the cold and warm models.

4 Discussion

4.1 Drivers of summer sea-ice extent

Our analysis suggests that both at the pan-Antarctic scale and sectoral scale, proximate factors, such as the previous spring sea-ice extent, SST and surface air temperature, are the most important drivers of changes in summer sea-ice extent over the historical and future periods (1970–2100) in the five large model ensembles analyzed here (Figs. 7, 8, 9, 10). SAM also displays some direct influence at the pan-Antarctic scale, in the Bellingshausen-Amundsen Seas, Weddell Sea, and Ross Sea, although the values of information transfer are small compared to proximate drivers. The ASL rarely directly influences summer sea-ice extent, but shows some indirect influence via SAM. Teleconnection patterns (ENSO and IOD) are most important in the Ross Sea and Western Pacific Ocean, while they are almost inexistent in other sectors. These results highlight the complexity of processes at play in the Southern Ocean that lead to changes in Antarctic summer sea-ice extent.

One of the mechanisms identified in previous studies to explain the recent changes in Antarctic summer sea-ice extent is an influence of SAM on the ASL (both being potentially impacted by ENSO and IOD), which then affects sea ice in the Bellingshausen-Amundsen and Ross Seas (Lefebvre et al. 2004; Turner et al. 2015; Eayrs et al. 2021; Zhang and Li 2023). The exact season when the effect of SAM and ASL on summer Antarctic sea ice is largest is not entirely clear, but spring (as used in our study) has been found to be relevant in several studies (Eayrs et al. 2021; Zhang and Li 2023; Wang et al. 2024). With our results, we do not find such a causal chain from SAM to ASL and then to summer Antarctic sea ice. We rather identify a more complex picture, where SAM and ASL indeed have some influence (especially in the Bellingshausen-Amundsen and Ross sectors, but not only), but they rather indirectly impact summer sea-ice extent via proximate factors, such as SST, previous sea-ice extent and surface air temperature. SAM and ASL are negatively correlated in all models (not shown), and ASL influences SAM in only two models (CanESM5 and EC-Earth3), with no reverse influence of SAM on ASL (Fig. 4). In these two models, there is no consensus on the resulting causal influence on summer sea-ice extent. In CanESM5, SAM directly influences summer Antarctic, Weddell and Ross sea-ice extent (Fig. 4b and Fig. 9), while it does not directly impact summer sea-ice extent at the pan-Antarctic scale and in any of the five sectors in EC-Earth3 (Fig. 4d and Fig. 10). Thus, the potential influence of ASL on SAM found in some models does not systematically impact the resulting influence on summer sea-ice extent.

4.2 Regional differences

In our study, we find that the Indian and Western Pacific Oceans generally display smaller values of direct causal influences on summer sea-ice extent, compared to other sectors (Fig. 7). This may be partly due to the generally less dense causal network in these sectors (Figs. 8-10 and A9–A10). This suggests that the behavior of sea ice in these two sectors is more unpredictable compared to the three other sectors. Further investigation would be needed to identify the reasons for such a behavior.

Additionally, we focused on intra-basin relationships in our analysis (e.g. influence of SST in the Weddell Sea on summer sea-ice extent in the Weddell Sea), but it could be the case that the dynamics in a basin influences another one (e.g. influence of SST in the Weddell Sea on summer sea-ice extent in the Indian Ocean). These inter-basin relationships could be the subject of a future study.

4.3 Model dependence

The three types of models (moderate, cold and warm models) do not behave in a highly distinct manner in terms of causal influences (Sect. 3.2.2). In order to more precisely quantify the impacts of the model mean state as well as its interannual variability (measured by standard deviation) on our results, we performed an additional analysis. Figure A11 displays the rates of information transfer as a function of the model mean state (first row) and model interannual variability (second row) over 1982–2023 to better compare to observations, which we also provide in this figure.

We find that the mean previous sea-ice extent might impact the influencing role of this variable on summer sea-ice extent, as a larger mean previous sea-ice extent (as in CanESM5) generally leads to a lower causal influence (Fig. A11a). However, observations stand outside this trend as they display a relatively large influence of the mean previous sea-ice extent for a relatively large mean sea-ice extent. While CESM2 and ACCESS-ESM1.5 are in good agreement with the observed mean previous sea-ice extent, the influence of the previous sea-ice extent is lower for these models compared to observations, and EC-Earth3 and MPI-ESM1.2-LR are closer to observations (Fig. A11a).

ACCESS-ESM1.5 and CESM2 are relatively close to the observed mean surface air temperature, but they present a causal influence of surface air temperature on summer sea-ice extent that is lower than observations (Fig. A11b). EC-Earth3 and MPI-ESM1.2-LR are indeed closer to observations in terms of the rate of information transfer from surface air temperature, despite having too large a mean surface air temperature.

The model closer to the mean observed SST is CanESM5, but it displays a rate of information transfer from SST to summer sea-ice extent of $|\tau| = 12\%$, while it is close to zero in observations (Fig. A11c). ACCESS-ESM1.5 also presents a causal influence close to zero, but its mean surface air temperature is more than $1\,^{\circ}$C larger than observations.

No clear impact of model interannual variability on causal influences is found (Fig. A11d-e). CESM2 is the closest model to observations in terms of interannual variability in previous sea-ice extent, surface air temperature and SST. While it presents a too low rate of information from the previous sea-ice extent (Fig. A11d) and from surface air temperature (Fig. A11e), it is relatively close to the observed causal influence of SST on summer sea-ice extent (Fig. A11f).

These results show that models closer to observations in terms of mean state or interannual variability are not necessarily closer to observations for causal influences. We insist that all observed rates of information are not statistically significant due to the presence of only 1 realization (vs. 40–50 ensemble members for the five models). Due to the small sample of observational data points, observed rates of information need to be taken with care, and a model deviation from observations in terms of causal influence is not defined as a bias here. We would need to have access to a much larger number of data points to provide insightful results in terms of observations.

In addition, previous studies have shown that although the models used here are affected by known biases in sea-ice extent and other climate variables, they have been proved to be useful tools to investigate different aspects of Antarctic sea-ice variability. For example, Espinosa et al. (2024) found that the CESM2 model nudged to observed winds can reproduce the observed record low winter sea-ice extent of 2023. Purich and England (2019) showed that the tropical Indian Ocean likely contributed to anomalous atmospheric circulation leading to the Antarctic sea-ice decline in spring 2016 based on model experiments carried out with the ACCESS1.0 model. Another study found that multi-decadal variability in Antarctic sea ice was triggered by SAM via a salinity-convection feedback using some of the CMIP6 models used here, i.e. CanESM5, MPI-ESM1.2-LR and CESM2 (Morioka et al. 2024a).

4.4 Advantages and limitations of the causal method

The Liang-Kleeman information flow method allows to go beyond classical correlation analyses by quantifying cause-effect relationships between variables (Liang 2021). It allows to remove spurious dependencies based on correlations (Docquier et al. 2024a). Its two key advantages compared to other causal methods are its direct derivation from first principles of information entropy and its relatively simple implementation based on the covariance matrix (Liang 2016, 2021). The method allows to take feedback loops into account; more details can be found in Smirnov (2022).

The method presents three main limitations. First, it assumes linearity: while the method has been tested and validated with nonlinear synthetic examples (e.g. Liang 2014, 2021) and in a wide range of climate studies (e.g. Liang 2014; Docquier et al. 2022; Hagan et al. 2022; Vannitsem and Liang 2022), some nonlinear processes could appear and thus would not be taken into account. A nonlinear extension of the method has been recently developed and applied in theoretical settings (Pires et al. 2024; Vannitsem et al. 2024), but it still needs to be properly implemented for real-world applications.

Second, the method assumes that time series are stationary. This problem is dealt with by removing the linear trend (ensemble mean removal for models and linear detrending for observations). However, we acknowledge that even after this detrending, the residuals are not perfectly stationary. To take the effect of the changing variability into account, we carried out an additional test at the pan-Antarctic scale by dividing the detrended data by the ensemble standard deviation for each model before computing rates of information transfer (Fig. A12). We found similar results to our original findings with detrended data (Fig. 3), with a small exception being a larger (and significant) influence of surface air temperature for EC-Earth3 (Fig. A12a). In our study, we prefer not to perform any additional data processing to introduce as few changes in the original data as possible, so we only perform a linear detrending.

Third, the method, like any other causal method, requires relatively long time series (at least 100 data points) to infer robust causal links. This may explain most of the non-significant causal links in observations. In our study, we focused on the interannual time scale, but repeating this analysis at monthly time scale would probably provide more statistically significant causal influences in observations due to the larger number of data points.

5 Conclusions

In our study, we used the Liang-Kleeman information flow method to identify the drivers of recent and future changes (1970–2100) in Antarctic summer-ice extent at interannual time scale, based on five CMIP6 large ensembles. We found that proximate drivers, such as the previous spring sea-ice extent, SST and surface air temperature, play a large role at the pan-Antarctic scale and in a majority of Antarctic sectors. An exception is the Western Pacific Ocean, where ENSO and IOD have a larger influence compared to other sectors, and proximate factors have a very limited effect. We also looked at observed causal influences, but results are mostly not statistically significant due to the short observational time period. Additionally, we find a general decrease of the previous sea-ice extent influence over time, together with an increasing SST impact along the years.

The analysis of causal networks for three different types of models (a moderate, a cold and a warm model) provides additional insights into the complexity of the processes at play in each region. All three types of models display a large SST influence in both the Bellingshausen-Amundsen and Weddell Seas. In the Indian Ocean, which presents the least dense causal network for all three types of models, the most important drivers are the previous sea-ice extent in the moderate model, SST in the cold model, and surface air temperature in the warm model. SST plays a large role in the moderate and warm models in the Western Pacific Ocean, while ENSO and IOD have more influence in the cold model for this sector. The teleconnection patterns (ENSO and IOD) are generally important in the Ross Sea. While SAM is not the largest actor in any region for any model, it shows an effect (mainly indirectly via SST) on summer sea-ice extent for the three types of models.

Finally, an interesting feature of our analysis is that the Western Pacific Ocean and Indian Ocean generally display weak values of causal influences compared to other sectors, and have a less dense causal network. This suggests that these two regions are more unpredictable from the standard variables selected here, and it would be beneficial to further investigate the reasons behind this distinct behavior. Additionally, inter-basin relationships could also be the subject of further analysis.

Supplementary Information The online version contains supplementary material available at https://doi.org/10.1007/s00382-025-07878-3.

Acknowledgements We thank the editor Susanna Corti, as well as Edward Doddridge and one anonymous reviewer for their comments, which helped us improve our article.

Author contributions D.D. led the work with contributions from F.M., B.R., T.F., H.G., B.M., D.T. and S.V. D.D. performed the computations, analyzed the results, produced the figures and led the paper writing. B.R. computed the OSTIA spatial mean. All authors participated in the design of the study, the interpretation of the results and the writing of the paper.

Funding This study is supported by the Belgian Science Policy Office (BELSPO) under the RESIST project (contract no. RT/23/RESIST). David Docquier and Benjamin Richaud were funded by BELSPO through the RESIST project. François Massonnet is a F.R.S.-FNRS Research Associate. Hugues Goosse is a F.R.S.-FNRS Research Director. Bianca Mezzina is a F.R.S.-FNRS postdoctoral researcher. Dániel Topál is a F.R.S.-FNRS Research Fellow.

Data availability All CMIP6 (Eyring et al. 2016) model outputs (except CESM2) used in this study (historical and SSP3−7.0 simulations) were retrieved from the Earth System Grid Federation (ESGF) nodes: https://esgf-index1.ceda.ac.uk/search/cmip6-ceda/. Table 1 provides the references of the model simulations used. CESM2 (Rodgers et al. 2021) model outputs were retrieved from the National Center for Atmospheric Research (NCAR) Climate Data Gateway: https://www.earthsystemgrid.org/dataset/ucar.cgd.cesm2le.output.html. The observed sea-ice extent from OSI SAF (OSI SAF 2023) can be accessed through the EUMETSAT repository: https://osi-saf.eumetsat.int/products/osi-420 (last access: 10 December 2024). The ERA5 (Hersbach et al. 2020) surface air temperature was retrieved from the Copernicus Climate Data Store: https://cds.climate.copernicus.eu/datasets/reanalysis-era5-single-levels-monthly-means?tab=overview (last access: 23 June 2025). The OSTIA data (Good et al. 2020) were accessed via the Copernicus portal: https://data.marine.copernicus.eu/product/SST_GLO_SST_L4_REP_OBSERVATIONS_010_011/description (last access: 25 October 2024). The observed SAM index (Marshall 2003) was retrieved from G. J. Marshall's website: https://legacy.bas.ac.uk/met/gjma/sam.html (last access: 29 January 2024). The observed ASL data (Hosking et al. 2016) are from S. Hosking's website: https://scotthosking.com/asl_index (last access: 6 December 2024). Niño3.4 and DMI observed data come from the NOAA Physical Sciences Laboratory: https://psl.noaa.gov/data/climateindices/list/ (last access: 26 June 2024).

Code availability The Python scripts to produce the figures of this article, including the functions to compute rates of information transfer, are available on Zenodo: https://doi.org/10.5281/zenodo.15819168 (Docquier 2025).

Declarations

Conflict of interest The authors have no Conflict of interest to declare that are relevant to the content of this article.

References

Bonan DB, Dörr J, Wills RCJ et al (2024) Sources of low-frequency variability in observed antarctic sea ice. Cryosphere 18(4):2141–2159. https://doi.org/10.5194/tc-18-2141-2024

Comiso JC, Parkinson CL, Gersten R, et al (2024) Current state of sea ice cover. https://earth.gsfc.nasa.gov/cryo/data/current-state-sea-ice-cover, last access: 12-13-2024

Ding Q, Steig EJ, Battisti DS et al (2012) Influence of the tropic on the southern annular mode. J Clim 25(18):6330–6348. https://doi.org/10.1175/JCLI-D-11-00523.1

Docquier D (2025) Codes related to the drivers of summer antarctic sea-ice extent based on information flow. Zenodo. https://doi.org/10.5281/zenodo.15819168

Docquier D, Vannitsem S, Ragone F, et al (2022) Causal links between Arctic sea ice and its potential drivers based on the rate of information transfer. Geophysical Research Letters 49(9):e2021GL095892. https://doi.org/10.1029/2021GL095892

Docquier D, Capua GD, Donner RV et al (2024) A comparison of two causal methods in the context of climate analyses. Nonlinear Process Geophys 31:115–136. https://doi.org/10.5194/npg-31-115-2024

Docquier D, Massonnet F, Ragone F, et al (2024b) Drivers of summer Arctic sea-ice extent at interannual time scale in CMIP6 large ensembles revealed by information flow. Scientific Reports 14(24236). https://doi.org/10.1038/s41598-024-76056-y

Doddridge EW, Marshall J (2017) Modulation of the seasonal cycle of antarctic sea ice extent related to the southern annular mode. Geophys Res Lett 44(19):9761–9768. https://doi.org/10.1002/2017GL074319

Eabry MD, Goyal R, Taschetto AS et al (2024) Combined impacts of southern annular mode and zonal wave 3 on antarctic sea ice variability. J Clim 37(5):1759–1775. https://doi.org/10.1175/JCLI-D-23-0516.1

Eayrs C, Li X, Raphael MN et al (2021) Rapid decline in antarctic sea ice in recent years hints at future change. Nat Geosci 14:460–464. https://doi.org/10.1038/s41561-021-00768-3

EC-Earth-Consortium (2019a) EC-Earth-Consortium EC-Earth3 model output prepared for CMIP6 CMIP historical. Version 20200412. https://doi.org/10.22033/ESGF/CMIP6.4700, Earth System Grid Federation

EC-Earth-Consortium (2019b) EC-Earth-Consortium EC-Earth3 model output prepared for CMIP6 ScenarioMIP ssp370. Version 20210101. https://doi.org/10.22033/ESGF/CMIP6.4884, Earth System Grid Federation

Espinosa ZI, Blanchard-Wrigglesworth E, Bitz CM (2024) Understanding the drivers and predictability of record low Antarctic sea ice in austral winter 2023. Communications Earth and Environment 5(723). https://doi.org/10.1038/s43247-024-01772-2

Eyring V, Bony S, A. G, et al (2016) Overview of the coupled model intercomparison project phase 6 (cmip6) experimental design and organization. Geoscientific Model Development 9(5):1937–1958. https://doi.org/10.5194/gmd-9-1937-2016

Ferreira D, Marshall J, Bitz CM et al (2015) Antarctic ocean and sea ice response to ozone depletion: a two-time-scale problem. J Clim 28(3):1206–1226. https://doi.org/10.1175/JCLI-D-14-00313.1

Fogt RL, Sleinkofer AM, Raphael MN et al (2022) A regime shift in seasonal total antarctic sea ice extent in the twentieth century. Nat Clim Chang 12:54–62. https://doi.org/10.1038/s41558-021-01254-9

Fox-Kemper B, Hewitt HT, Xiao C, et al (2021) Ocean, Cryosphere and Sea Level Change. In: Climate Change 2021: The Physical Science Basis. Contribution of Working Group I to the Sixth Assessment Report of the Intergovernmental Panel on Climate Change [Masson-Delmotte, V., P. Zhai, A. Pirani, S. L. Connors, C. Péan, S. Berger, N. Caud, Y. Chen, L. Goldfarb, M. I. Gomis, M. Huang, K. Leitzell, E. Lonnoy, J. B. R. Matthews, T. K. Maycock, T. Waterfield, O. Yelekçi, R. Yu and B. Zhou (eds.)]. Cambridge University Press, Cambridge, United Kingdom and New York, NY, USA, https://doi.org/10.1017/9781009157896.011

Gilbert E, Holmes C (2024) 2023's antarctic sea ice extent is the lowest on record. Weather 79(2):46–51. https://doi.org/10.1002/wea.4518

Gong D, Wang S (1999) Definition of antarctic oscillation index. Geophys Res Lett 26(4):459–462. https://doi.org/10.1029/1999GL900003

Good S, Fiedler E, Mao C, et al (2020) The current configuration of the OSTIA system for operational production of foundation sea surface temperature and ice concentration analyses. Remote Sensing 12(4). https://doi.org/10.3390/rs12040720

Hagan DFT, Dolman HAJ, Wang G et al (2022) Contrasting ecosystem constraints on seasonal terrestrial CO_2 and mean surface air temperature causality projections by the end of the 21st century. Environ Res Lett 17:124019. https://doi.org/10.1088/1748-9326/aca551

Hersbach H, Bell B, Berrisford P et al (2020) The era5 global reanalysis. Q J R Meteorol Soc 146(730):1999–2049. https://doi.org/10.1002/qj.3803

Hobbs W, Spence P, Meyer A et al (2024) Observational evidence for a regime shift in summer antarctic sea ice. J Clim 37(7):2263–2275. https://doi.org/10.1175/JCLI-D-23-0479.1

Hosking JS, Orr A, Bracegirdle TJ et al (2016) Future circulation changes off west antarctica: sensitivity of the amundsen sea low to projected anthropogenic forcing. Geophys Res Lett 43(1):367–376. https://doi.org/10.1002/2015GL067143

Jena B, Kshitija S, Bajish CC, et al (2024) Evolution of Antarctic sea ice ahead of the record low annual maximum extent in September 2023. Geophysical Research Letters 51:e2023GL107561. https://doi.org/10.1029/2023GL107561

Lavergne T, Sorensen AM, Kern S et al (2019) Version 2 of the eumetsat osi saf and esa cci sea-ice concentration climate data records. Cryosphere 13:49–78. https://doi.org/10.5194/tc-13-49-2019

Lefebvre W, Goosse H, Timmermann R, et al (2004) Influence of the Southern Annular Mode on the sea ice–ocean system. Journal of Geophysical Research: Oceans 109(C9). https://doi.org/10.1029/2004JC002403

Liang XS (2014) Unraveling the cause-effect relation between time series. Phys Rev E 90:052150. https://doi.org/10.1103/PhysRevE.90.052150

Liang XS (2016) Information flow and causality as rigorous notions ab initio. Phys Rev E 94(5):052201. https://doi.org/10.1103/PhysRevE.94.052201

Liang XS (2021) Normalized multivariate time series causality analysis and causal graph reconstruction. Entropy 23(6):679. https://doi.org/10.3390/e23060679

Liang XS, Kleeman R (2005) Information transfer between dynamical system components. Phys Rev Lett 95(24):244101. https://doi.org/10.1103/PhysRevLett.95.244101

Liu J, Zhu Z (2024) Projected Antarctic sea ice change contributes to increased occurrence of strong El Niño. npj Climate and Atmospheric Science 7(233). https://doi.org/10.1038/s41612-024-00789-w

Maksym T (2019) Arctic and antarctic sea ice change: contrasts, commonalities, and causes. Ann Rev Mar Sci 11:187–213. https://doi.org/10.1146/annurev-marine-010816-060610

Marshall GJ (2003) Trends in the southern annular mode from observations and reanalyses. J Clim 16(24):4134–4143. https://doi.org/10.1175/1520-0442(2003)016%3C4134:TITSAM%3E2.0.CO;2

Meehl GA, Arblaster JM, Chung CTY, et al (2019) Sustained ocean changes contributed to sudden Antarctic sea ice retreat in late 2016. Nature Communications 10(14). https://doi.org/10.1038/s41467-018-07865-9

Mezzina B, Goosse H, Huot PV et al (2024) Contributions of atmospheric forcing and ocean preconditioning in the 2016 antarctic sea ice extent drop. Environmental Research Climate 3:021002. https://doi.org/10.1088/2752-5295/ad3a0b

Mezzina B, Goosse H, Klein F et al (2024) The role of atmospheric conditions in the antarctic sea ice extent summer minima. Cryosphere 18(8):3825–3839. https://doi.org/10.5194/tc-18-3825-2024

Morioka Y, Manabe S, Zhang L, et al (2024a) Antarctic sea ice multidecadal variability triggered by Southern Annular Mode and deep convection. Communications Earth and Environment 5(633). https://doi.org/10.1038/s43247-024-01783-z

Morioka Y, Zhang L, Cooke W, et al (2024b) Role of anthropogenic forcing in Antarctic sea ice variability simulated in climate models. Nature Communications 15(10511). https://doi.org/10.1038/s41467-024-54485-7

Olonscheck D, Suarez-Gutierrez L, Milinski S, et al (2023) The New Max Planck Institute Grand Ensemble with CMIP6 forcing and high-frequency model output. Journal of Advances in Modeling Earth Systems 15(10):e2023MS003790. https://doi.org/10.1029/2023MS003790

OSI SAF (2023) EUMETSAT Ocean and Sea Ice Satellite Application Facility sea ice index 1978-onwards, version 2.2, OSI-420, Data extracted from OSI SAF FTP server: 1979-2024, Northern Hemisphere, accessed 2024-12-10. https://doi.org/10.15770/EUM_SAF_OSI_0022

Pires CA, Docquier D, Vannitsem S (2024) A general theory to estimate information transfer in nonlinear systems. Physica D: Nonlinear Phenomena 458(133988). https://doi.org/10.1016/j.physd.2023.133988

Purich A, Doddridge EW (2023) Record low Antarctic sea ice coverage indicates a new sea ice state. Communications Earth and Environment 4(314). https://doi.org/10.1038/s43247-023-00961-9

Purich A, England MH (2019) Tropical teleconnections to antarctic sea ice during austral spring 2016 in coupled pacemaker experiments. Geophys Res Lett 46(12):6848–6858. https://doi.org/10.1029/2019GL082671

Raphael MN, Hobbs W (2014) The influence of the large-scale atmospheric circulation on antarctic sea ice during ice advance and retreat seasons. Geophys Res Lett 41(14):5037–5045. https://doi.org/10.1002/2014GL060365

Raphael MN, Maierhofer TJ, Fogt RL, et al (2025) A twenty-first century structural change in Antarctica's sea ice system. Communications Earth and Environment 6(131). https://doi.org/10.1038/s43247-025-02107-5

Roach LA, Meier WN (2024) Sea ice in 2023. Nature Reviews Earth and Environment 5:235–237. https://doi.org/10.1038/s43017-024-00542-0

Roach LA, Dörr J, Holmes CR, et al (2020) Antarctic sea ice area in CMIP6. Geophysical Research Letters 47(9):e2019GL086729. https://doi.org/10.1029/2019GL086729

Rodgers KB, Lee SS, Rosenbloom N et al (2021) Ubiquity of human-induced changes in climate variability. Earth System Dynamics 12:1393–1411. https://doi.org/10.5194/esd-12-1393-2021

Runge J, Bathiany S, Bollt E et al (2019) Inferring causation from time series in earth system sciences. Nat Commun 10:2553. https://doi.org/10.1038/s41467-019-10105-3

Runge J, Gerhardus A, Varando G et al (2023) Causal inference for time series. Nature Reviews Earth and Environment 4:487–505. https://doi.org/10.1038/s43017-023-00431-y

Schroeter S, O'Kane TJ, Sandery PA (2023) Antarctic sea ice regime shift associated with decreasing zonal symmetry in the southern annular mode. Cryosphere 17(2):701–717. https://doi.org/10.5194/tc-17-701-2023

Shu Q, Qiao F, Song Z et al (2012) Sea ice trends in the antarctic and their relationship to surface air temperature during 1979–2009. Clim Dyn 38:2355–2363. https://doi.org/10.1007/s00382-011-1143-9

Smirnov DA (2022) Generative formalism of causality quantifiers for processes. Physical Review E 105(034209). https://doi.org/10.1103/PhysRevE.105.034209

Stuecker MF, Bitz CM, Armour KC (2017) Conditions leading to the unprecedented low antarctic sea ice extent during the 2016 austral spring season. Geophys Res Lett 44(17):9008–9019. https://doi.org/10.1002/2017GL074691

Sugihara G, May R, Ye H et al (2012) Detecting causality in complex ecosystems. Science 338(6106):496–500. https://doi.org/10.1126/science.1227079

Swadling KM, Constable AJ, Fraser AD et al (2023) Biological responses to change in antarctic sea ice habitats. Front Ecol Evol 10:1073823. https://doi.org/10.1038/s41612-024-00789-w

Swart NC, Cole JNS, Kharin VV, et al (2019a) CCCma CanESM5 model output prepared for CMIP6 CMIP historical. Version 20190429. https://doi.org/10.22033/ESGF/CMIP6.3610, Earth System Grid Federation

Swart NC, Cole JNS, Kharin VV, et al (2019b) CCCma CanESM5 model output prepared for CMIP6 ScenarioMIP ssp370. Version 20190429. https://doi.org/10.22033/ESGF/CMIP6.3690, Earth System Grid Federation

Swart NC, Cole JNS, Kharin VV et al (2019) The canadian earth system model version 5 (canesm5.0.3). Geoscientific Model Development 12:4823–4873. https://doi.org/10.5194/gmd-12-4823-2019

Turner J, Hosking JS, Bracegirdle TJ et al (2015) Recent changes in antarctic sea ice. Philos Trans R Soc 373(2045):20140163. https://doi.org/10.1098/rsta.2014.0163

Tyrovolas M, Liang XS, Stylios C (2023) Information flow-based fuzzy cognitive maps with enhanced interpretability. Granular Computing 18:2021–2038. https://doi.org/10.1007/s41066-023-00417-7

Vannitsem S, Liang XS (2022) Dynamical dependencies at monthly and interannual time scales in the climate system: Study of the North Pacific and Atlantic regions. Tellus A 74:141–158. https://doi.org/10.16993/tellusa.44

Vannitsem S, Dalaiden Q, Goosse H (2019) Testing for dynamical dependence: application to the surface mass balance over antarctica. Geophys Res Lett 46(21):12125–12135. https://doi.org/10.1029/2019GL084329

Vannitsem S, Pires CA, Docquier D (2024) Causal dependencies and shannon entropy budget: analysis of a reduced-order atmospheric model. Q J R Meteorol Soc 150(764):4066–4085. https://doi.org/10.1002/qj.4805

Vannitsem S, Docquier D, Wauthy S, et al (2025) Sources of low-frequency δ^{18}O variability in coastal ice cores from Dronning Maud Land (Antarctica). Climate Dynamics 63(48). https://doi.org/10.1007/s00382-024-07514-6

Wang J, Luo H, Yu L et al (2023) The impacts of combined sam and enso on seasonal antarctic sea ice changes. J Clim 36:3553–3569. https://doi.org/10.1175/JCLI-D-22-0679.s1

Wang J, Massonnet F, Goosse H, et al (2024) Synergistic atmosphere-ocean-ice influences have driven the 2023 all-time Antarctic sea-ice record low. Communications Earth and Environment 5(415). https://doi.org/10.1038/s43247-024-01523-3

Wieners KH, Giorgetta M, Jungclaus J, et al (2019a) MPI-M MPI-ESM1.2-LR model output prepared for CMIP6 CMIP historical. Version 20190710. https://doi.org/10.22033/ESGF/CMIP6.6595, Earth System Grid Federation

Wieners KH, Giorgetta M, Jungclaus J, et al (2019b) MPI-M MPI-ESM1.2-LR model output prepared for CMIP6 ScenarioMIP ssp370. Version 20190710. https://doi.org/10.22033/ESGF/CMIP6.6695, Earth System Grid Federation

Wyser K, Koenigk T, Fladrich U et al (2021) The smhi large ensemble (smhi-lens) with ec-earth3.3.1. Geoscientific Model Development 14:4781–4796. https://doi.org/10.5194/gmd-14-4781-2021

Ye Z, Tozuka T (2022) Causal relationship between sea surface temperature and precipitation revealed by information flow. Frontiers in Climate 4(1024384). https://doi.org/10.3389/fclim.2022.1024384

Zhang C, Li S (2023) Causes of the record-low antarctic sea-ice in austral summer 2022. Atmospheric and Oceanic Science Letters 16(6):100353. https://doi.org/10.1016/j.aosl.2023.100353

Zhang L, Delworth TL, Yang X, et al (2022) The relative role of the subsurface Southern Ocean in driving negative Antarctic Sea ice extent anomalies in 2016–2021. Communications Earth and Environment 3(302). https://doi.org/10.1038/s43247-022-00624-1

Zhang L, Ren X, Cai W, et al (2024) Weakened western Indian Ocean dominance on Antarctic sea ice variability in a changing climate. Nature Communications 15(3261). https://doi.org/10.1038/s41467-024-47655-0

Zhou S, Meijers AJS, Meredith MP et al (2023) Slowdown of antarctic bottom water export driven by climatic wind and sea-ice changes. Nat Clim Chang 13:701–709. https://doi.org/10.1038/s41558-023-01695-4

Ziehn T, Chamberlain M, Lenton A, et al (2019a) CSIRO ACCESS-ESM1.5 model output prepared for CMIP6 CMIP historical. Version 20200803. https://doi.org/10.22033/ESGF/CMIP6.4272, Earth System Grid Federation

Ziehn T, Chamberlain M, Lenton A, et al (2019b) CSIRO ACCESS-ESM1.5 model output prepared for CMIP6 ScenarioMIP ssp370. Version 20210624. https://doi.org/10.22033/ESGF/CMIP6.4324, Earth System Grid Federation

Ziehn T, Chamberlain MA, Law RM et al (2020) The australian earth system model: access-esm1.5. Journal of Southern Hemisphere Earth Systems Science 70:193–214. https://doi.org/10.1071/ES19035

Zwally HJ, Comiso JC, Parkinson CL, et al (1983) Antarctic sea ice, 1973–1976: Satellite passive-microwave observations, vol 459. NASA Special Publication, Washington D.C